Overdamped stress relaxation in buckled rods

Oskar Hallatschek, Erwin Frey, and Klaus Kroy
Hahn-Meitner Institut, Glienicker Straße 100, D-14109 Berlin, Germany
and Fachbereich Physik, Freie Universität Berlin, Arnimallee 14, D-14195 Berlin, Germany
(Received 3 February 2004; published 15 September 2004)

We present a comprehensive theoretical analysis of the stress relaxation in a multiply but weakly buckled incompressible rod in a viscous solvent. For the bulk, two interesting parameter regimes of generic self-similar intermediate asymptotics are distinguished, which give rise to approximate and exact power-law solutions, respectively. For the case of open boundary conditions the corresponding nontrivial boundary-layer scenarios are derived by a multiple-scale perturbation ("adiabatic") method. Our results compare well with—and provide the theoretical explanation for—previous results from numerical simulations, and they suggest directions for further fruitful numerical and experimental investigations.

DOI: 10.1103/PhysRevE.70.031802 PACS number(s): 36.20.−r, 61.41.+e

I. INTRODUCTION

Any child that has played with a ruler during a boring school lesson has experienced the diverting physics of the paradigm of a mechanical instability: the sudden buckling of a slender rod under a compressive axial load of weight f surpassing the first critical Euler force f_1. This so called Euler buckling instability is not only a well-known example of a simple mechanical system exhibiting nontrivial elastic behavior, historically it is also associated with the beginning of bifurcation theory. Its thorough understanding can temper our intuition as to what should be expected or searched after in more complicated situations involving elastic instabilities or bifurcations in general. Intriguingly, it has also proved to be of major importance for the equilibrium thermodynamic properties of stiff biopolymers [1,2], such as actin or collagen, which are largely responsible for the elastic properties of biological tissue. Recently the dynamics of the Euler instability has also gained considerable interest as one of the most elementary elastohydrodynamic problems [3]. The latter are commonly encountered in the derivation of macroscopic constitutive models for soft, viscoelastic materials, i.e., materials that show a mixed elastic and viscous behavior. For major examples of this important type of condensed matter, ranging from polymer solutions and gels to biological cells, the complicated dynamic response can indeed be attributed to the elastohydrodynamics of some low-dimensional mesoscale structures [4–6]. Thus the focus has shifted away from the classical treatment of the Euler instability [7], which is motivated by typical engineering problems such as the stability of a mechanical beam under compressive loads, to thermally undulated rods. A crucial difference between the two situations is that usually only the first few Euler modes matter in the former, whereas (infinitely) many modes are excited in the latter.

In the present contribution we are interested in deterministic ("athermal") dynamics under circumstances where many modes contribute. Despite this restriction, our methods and major results are also pertinent to certain "thermal" problems. A telling example is provided by the successful application of scaling arguments based on deterministic dynamics to rationalize the nonequilibrium longitudinal response of a semiflexible polymer [8–10]. More precisely, we will consider here the deterministic overdamped relaxation of the tension in an incompressible buckled rod as schematically depicted in Fig. 1. Initially, the contour is strongly wrinkled on short length scales, causing the end-to-end distance $R(t=0) \lesssim L$ to slightly deviate from the contour length L. It then evolves in time toward a completely straight final state $R(t \to \infty) = L$ by transferring contour length "stored" in the high Euler modes to successively lower modes with fewer and fewer nodes. The elastic energy stored in the compressed initial state is thereby dissipated to the solvent. The athermal case already exhibits a very rich phenomenology (emergence of a characteristic wavelength, exact and approximate power-law relaxation, helix formation, staircase relaxation), only some of which has previously been observed in numerical simulations [11,12]. These earlier studies also provided scaling arguments rationalizing some of the observations on the basis of a mathematical description adapted to the simulation technique, which involves a compressible rod. In contrast, our analysis starts from the math-

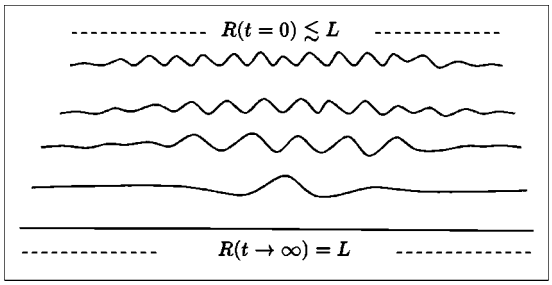

FIG. 1. A typical scenario of a deterministically relaxing buckled rod. Initially the rod is wrinkled on small wavelengths. In the course of time undulations are pushed out at the free ends and the typical wavelength of the undulations grows.

ematical minimal model[1] for the various phenomena of interest outlined above, which is a contour $\mathbf{r}(s,t)$ parametrized by its arc length $s=0,\ldots,L$ and subject to an energetic cost

$$\mathcal{H}_0[\mathbf{r}(s)] = \frac{\kappa}{2}\int_0^L ds\mathbf{r}''(s)^2 \tag{1}$$

for bending that is proportional to the square of the local curvature $\mathbf{r}''(s)$ (where we have introduced the shorthand notation $\mathbf{r}' \equiv \partial\mathbf{r}/\partial s$). The local incompressibility of the contour has to be imposed onto Eq. (1) as an external rigid constraint

$$\mathbf{r}'(s)^2 = 1, \tag{2}$$

which considerably complicates the calculations compared to classical polymer models with fluctuating contour length [13]. For finite temperatures, this model is generally known as the Kratky-Porod model or wormlike-chain model in the polymer literature [13,14]. However, as we said, here we focus on its deterministic (zero-temperature) dynamics, exclusively. The contour is embedded into a highly viscous solvent of viscosity η, and in the low-Reynolds-number and free-draining limit one approximates the viscous friction (per length) of a slender rod of thickness $a \ll L$ by two coefficients $\zeta_\perp = 2\zeta_\parallel \approx 4\pi\eta/\ln(L/a)$ for transverse and longitudinal motion relative to the solvent, respectively [13].

We emphasize that a crucial ingredient implicit in related earlier studies is the weakly-bending-rod limit. It asserts that the local slope of the contour is small. This condition has to be met for a large negative line tension (pressure) $f \gg f_1$ to build up along the contour. (Formally f plays the role of a Lagrange multiplier enforcing the incompressibility constraint onto $\mathcal{H}_0$.) Moreover, the condition of weak bending naturally provides a small parameter

$$\epsilon \equiv 1 - R(t=0)/L \ll 1, \tag{3}$$

the fraction of the contour length initially "stored" in the contour undulations. Technically, the existence of this small parameter is vital for the analytical approach to the problem. It enables us to establish two independent mechanisms behind the ubiquitous [11,12] power-law temporal decay of the tension

$$f(t) \propto t^{-1/2}. \tag{4}$$

We will show that Eq. (4) generically emerges as a consequence of two types of initial conditions (referred to as type I and type II). It will turn out that in the first case the structural relaxation proceeds hand in hand with tension relaxation, whereas in the second case it occurs essentially stress-free, after the tension has already relaxed. In both cases, we will also derive the associated growth laws for the boundary layers near free ends and analyze their contribution to the relaxation of the rod. The required adiabatic method of slowly varying tension, which we develop in Sec. V B and in the Appendix, can be generalized to stochastic dynamics [15] and thus provides a conceptional basis for a unifying description of tension propagation in slender rods. The scenarios established for the tension relaxation entail corresponding power-law scenarios for a number of observables such as the dissipated energy or the growth of the radius of gyration or end-to-end distance, which will be compared to simulations where available.

The remainder is organized as follows. In the next section, we further specify the problem and give some intuitive arguments as to its mathematical structure and the expected dynamics. For those readers who happen to be mainly interested in a qualitative overview of the rich deterministic dynamics of the Euler instability, we moreover give a comprehensive qualitative and phenomenological discussion of the results. Section II can also be read as an extensive introduction to and outline of the detailed calculations and results reported in the subsequent sections and in the Appendix.

II. QUALITATIVE DISCUSSION

The classical analysis [7] of the statics of beam buckling determines the onset of buckling from a linear stability analysis. More precisely, after decomposing the rod contour into discrete Fourier modes with amplitudes a_n, it yields the associated critical forces $f_n = \kappa(\pi n/L)^2$ (here for the case of hinged ends) necessary to excite these modes. If only the mode n is excited the corresponding bending energy as a function of the relative compression ϵ follow as $\mathcal{H}_0(\epsilon) = f_n L\epsilon$ in the weakly bending limit. One may hope that also the *dynamics* of the instability should be accessible to an essentially linear calculation for a weakly bending rod, although the problem outlined above is intrinsically nonlinear. We will show below that this is indeed the case as long as the tension along the rod is sufficiently uniform. Then the dynamics can be understood as arising from a linear superposition of relaxing eigenmodes that are only *globally* coupled by the incompressibility constraint Eq. (2). It restrains exponential growth of the unstable modes by selecting the intermediate asymptotic power-law relaxation Eq. (4) of the tension $f(t)$.

Although our mathematical analysis applies more generally, it is instructive to take the example of a free rod with a special initial condition as a starting point; namely a contour that is wrinkled at short scales with wrinkles that are statistically uniform along the whole contour. Obviously the relaxation at the free ends will not be the same as in the bulk, but for the time being we concentrate on the bulk behavior. Take an arbitrarily chosen short segment of length l far away from the rod ends. To fully relax its bending energy it would have to release its stored length $\varrho^0 l \approx \epsilon l$ and thus to expand. To this end, the sections of the rod to both of its sides would have to be pushed out. Since these were assumed to be very long and almost straight, so that their displacement is subject to substantial viscous friction from the embedding fluid, this is virtually impossible for a considerable period of time. (Note that the assumption of an almost straight contour is

[1] In contrast to related studies on two-dimensional membranes [4], where a finite "backbone" compressibility is in fact a necessary ingredient, it does not play a vital role for the various phenomena of interest in the present contribution. However, we note that in the simulation studies in Refs. [11,12], it provided a convenient means for the preparation of rods in an excited state giving rise to the "cascading scenario" discussed in Sec. IV C.

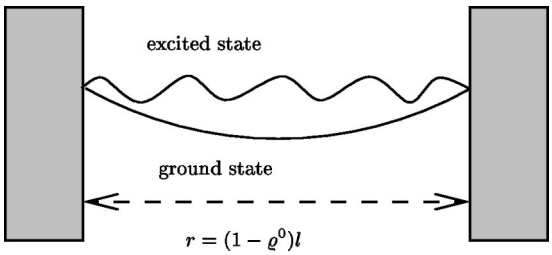

FIG. 2. Relaxation in the bulk. The situation is essentially the same as for a longitudinally confined rod. The pressure $f(t)$ exerted onto the confining walls exhibits the power-law decay Eq. (4).

crucial at this point.) The chosen initial condition therefore entails that a uniform axial pressure f much larger than the critical pressure f_1 for the ground state builds up along the contour. For a first analysis we may therefore imagine the chosen bulk section of the rod to be caged between two immobile boundaries of distance $r=(1-\varrho^0)l$ that preserves its total stored length

$$\varrho^0 l = l - r = \text{const}, \tag{5}$$

as depicted in Fig. 2 and analyzed in Sec. IV. The initial pressure $f(t=0)$ within the section (which is the negative of the force exerted onto the boundaries) can however still relax by transferring stored length from high modes to low modes. For the sake of the argument, we imagine the initial conformation to have essentially the form of a sine function with a very small wavelength. In other words, the mode amplitudes $a_n(0)$ will be peaked around some $N \gg 1$ in mode space, say, all $a_{n<N}$ are extremely small and all $a_{n>N}$ vanish identically. Then the initial pressure f_N is much higher than the final (ground state) pressure f_1. It will therefore relax by transferring the conserved stored length $\varrho^0 l$ from the Nth mode to successively lower modes, thereby dissipating stored elastic energy to the solvent. Since lower modes have longer relaxation times they evolve more slowly, and the transfer of stored length happens via a *cascade in mode space* involving all intermediate modes. It turns out that the initial localization of stored length and bending energy in mode space is not lost. The numerical solution in Sec. IV C will explicitly confirm that under such conditions the transfer actually occurs in a discontinuous jump mode leading to a staircase relaxation of the line tension $f(t)$ and the corresponding confinement force around the power law Eq. (4). Further, we will demonstrate analytically that the localization in mode space emerges asymptotically for certain initial conditions (notably those to be classified as type I below). We will discuss in detail how the global coupling of the modes via the constraint for the end-to-end distance r selects up to logarithmic corrections the power-law decay Eq. (4) as intermediate asymptotics. It will be shown that the localization in mode space consecutively sharpens with time, thereby establishing the above mentioned staircase relaxation as a generic long-time feature for those initial conditions. The mechanism behind the localization in mode space will be seen to be formally analogous to the onset of phase separation after a deep quench, i.e., to the early stages of spinodal decomposition [16,17].

A more thorough analysis of the initial conditions giving rise to power-law relaxation in the bulk will be performed in Secs. IV D and IV E. The key observation is that apart from the just mentioned cascading in mode space, there is another mechanism leading to similarity solutions *exactly* obeying Eq. (4). Contrary to the cascading solutions, where Eq. (4) can be understood as the immediate consequence of the appearance of a time-dependent characteristic wavelength

$$Q^{-1}(t) \propto t^{1/4} \tag{6}$$

that visibly dominates the contour undulations, no palpable dominant length scale (and hence no generic staircase relaxation) develops for this second class of solutions. In fact, hardly any conformational relaxation is noticeable during tension relaxation, and the structural dynamics is predominantly stress-free in this case. Dynamic scaling simply arises as a consequence of the *self-affine geometry* of the initial conditions characterized by a power-law distribution of the initial mode amplitudes $a_n(0) \propto n^{-\beta/2-1}$ with a "roughness exponent" $1<\beta<3$. Among these is the particularly interesting "thermally" undulated contour ($\beta=2$, the dynamics still supposed to be athermal). By restricting the discussion to power-law initial conditions with a mode cutoff to respect Eq. (3), a precise classification of initial conditions is possible. Power-law initial conditions with $\beta<1$ are then said to be of type I (they give rise to "cascading" solutions), and those with $1<\beta<3$ of type II (they give rise to exact similarity solutions). The case $\beta>3$ can be dismissed, because it amounts to situations where essentially all stored length is initially contained in the lowest mode. The discussion in Secs. IV C and IV D will eventually allow us to conclude in Sec. IV E that all *generic*[2] initial conditions invariably give rise to the same universal power-law relaxation Eq. (4) of the force but with variable degree of localization in mode space, as summarized in Fig. 7 below.

While the discussion so far holds anywhere in the bulk of the rod, where the longitudinal expansion can essentially be neglected on the appropriate logarithmic time scale, we will in the remainder also address the slightly different situation near the free ends (Sec. V). Surprisingly, it can be analyzed along the same lines as the bulk by virtue of a length scale separation innate to the weakly bending limit. The major variation of the tension, namely, from its bulk value to zero at the open boundaries, occurs within a (time-dependent) *boundary layer* of length $\lambda(t)$ that is at any time much larger than the characteristic length scale $Q^{-1}(t)$ of the dynamically most active contour undulations. This fortunate situation is schematically depicted in Fig. 9 below. It allows the derivation of closed equations for the (smooth) coarse-grained tension profile by means of an adiabatic approximation that integrates out the contingent short-wavelength fluctuations up

[2]Although our discussion is qualitatively valid also for initial conditions that deviate from ideal power-law distributions, we want to discard as "nongeneric" those initial conditions where one either starts essentially in the ground state ($\beta>3$) or has multiple peaks, oscillations, etc. in the mode spectrum. This attitude is commonly adopted in related studies [8,9].

to a coarse-graining length scale $l(t)$ intermediate between $Q^{-1}(t)$ and $\lambda(t)$. The underlying idea goes back to Ref. [8]. As an aside, we point out a subtle technical difference between the bulk and the boundary-layer problem, here. While the former is accessible to an ordinary (regular) perturbative approach, the adiabatic approach to the latter amounts to a multiple-scale perturbation scheme. The additional effort is rewarded by the possibility to generalize the approach to arbitrary situations that exhibit a slow (compared to l) "systematic" variation of the line tension and stored length along the contour. The corresponding formalism is developed in Sec. V B and the Appendix and enables us to derive the central Eq. (65). It can be interpreted as a continuity equation for the (coarse-grained) local stored length, which generalizes Eq. (5) to situations with spatially varying tension $f(s)$. The application to the situation near the free ends allows us to infer a nontrivial dynamic scaling law for the boundary layer. Its width λ is found to grow according to

$$\lambda(t) \propto t^{\delta}. \tag{7}$$

The exponent δ characterizing this growth depends on the degree of localization of the stored length in mode space, so that one again has to distinguish between type I and type II initial conditions. For type I initial conditions we find $\delta = 1/4$; hence the boundary-layer width is proportional to (though numerically much larger than) the wavelength of the dominant mode, i.e., $\lambda \propto Q^{-1}$. It thus does not represent a new characteristic dynamic length scale itself. As we noticed for the bulk, tension propagation and contour relaxation proceed in parallel. Asymptotically the rod contour can be decomposed into a bulk region with homogeneous line tension $f(s) = \text{const}$ and two virtually stretched end sections where the tension has relaxed to the linear profile $f(s) \propto \eta s$ characteristic of a rigid rod subject to a viscous friction force. These predictions compare well with the available numerical simulations [12]. In contrast, for type II initial conditions, which have not yet been studied in simulations, $\delta = (3 - \beta)/8$ is predicted to depend on the roughness exponent β, so that λ provides a new (β-dependent) characteristic dynamic length scale in addition to Q^{-1}. The vanishing of δ for $\beta \to 3$ heralds the (trivial) limit of instant equilibration. For $1 < \beta < 3$ tension propagation precedes contour relaxation, so that most of the contour relaxation occurs under vanishing tension. Such curious dependence of relaxation behavior for type II initial conditions on the value of the exponent β was previously noticed in a different context [8,9]. As an important special case, we obtain the exponent $\delta = 1/8$ for "thermal" initial conditions, which coincides with the corresponding exponent for the nonequilibrium thermodynamic tension propagation known from linear response calculations [5,18].

The divergence of tension decay (or propagation) and conformational relaxation for type II initial conditions raises the question of how under these circumstances tension propagation can be observed in experiments or simulations. In Sec. VI we establish that the growth velocity of the longitudinal component $R_{G\|}$ of the radius of gyration of a weakly bending rod is generally proportional to the tension $f(t)$ in the "bulk" of the polymer,

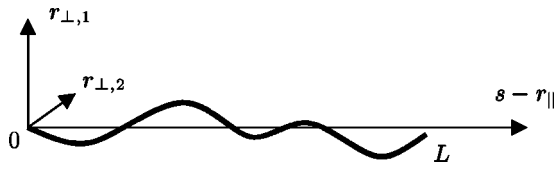

FIG. 3. The parameterization of the contour $\mathbf{r}(s) = (\mathbf{r}_{\perp}, s - r_{\|})^T$ by transverse and longitudinal displacement variables $r_{\perp}$ and $r_{\|}$, respectively. Note that the displacements vanish for the straight contour.

$$\partial_t R_{G\|}(t) \propto f(t). \tag{8}$$

Thus $R_{G\|}$ represents a suitable observable to directly monitor the decay law Eq. (4) for the tension $f(t)$. This said, $R_{G\|}$ obviously should not be regarded as a genuine measure of the conformational dynamics. The latter can instead be accessed via measuring the change $\delta R_{\|}(\tau)$ of the longitudinal component of the end-to-end distance. Because of its sensitivity to the boundary-layer width λ, it portrays the richer conformational dynamics in its power-law growth

$$\delta R_{\|}(t) \propto t^{\gamma}. \tag{9}$$

For type I initial conditions, $\delta R_{\|}$ is just a (small) constant fraction of the boundary layer width, i.e., $\delta R_{\|} \propto \lambda \propto Q^{-1}$, so that $\gamma = 1/4$. On the other hand, for type II initial conditions, Q^{-1}, λ, and $\delta R_{\|}$ all constitute different dynamic length scales, and we find a crossover from $\gamma = (1+\beta)/8 = \delta + (\beta - 1)/4$ for short times to $\gamma = (\beta - 1)/4$ for long times.

The above qualitative discussion has hopefully convinced the reader that the dynamics of the mechanical Euler buckling instability exhibits a rich and interesting phenomenology that deserves a more detailed mathematical analysis. This is what the following sections intend to provide.

III. EQUATIONS OF MOTION

As motivated in the Introduction, the axial incompressibility can lead to a large negative tension (pressure) in a relaxing rod. This crucial feature appears only for almost straight rods or straight rod sections, for which the fraction ϵ of initially stored length provides a small parameter. We therefore concentrate on the geometry of an almost straight rod and introduce displacement variables that describe the deviation from the straight contour, as depicted in Fig. 3. We parametrize the contour by $\mathbf{r} = (\mathbf{r}_{\perp}, s - r_{\|})^T$, where $\mathbf{r}_{\perp}(s)$ is the two-dimensional transverse displacement vector at arclength s and $r_{\|}(s) - r_{\|}(0)$ is the contour length stored in undulations within the rod section $(0, s)$.

The function $r'_{\|}(s,t)$ can be interpreted as the fraction of the contour length that is *locally* stored in the transverse undulations. As it turns out to be the density of a locally conserved quantity it will have central importance in our analysis. For convenience of notation we reserve the variable $\varrho(s,t)$ for it,

$$\varrho(s,t) \equiv r'_{\|}(s,t). \tag{10}$$

The spatial average

$$\int_0^L \frac{ds}{L}\varrho(s,0) = \epsilon \tag{11}$$

relates ϱ to the small parameter ϵ, defined in Eq. (3). The limit $\epsilon \to 0$ with $\varrho(s,0)/\epsilon$ fixed is called the *weakly bending limit* because it guarantees an almost straight contour,

$$\varrho(s,t) = O(\epsilon) \ll 1 \text{ (weakly bending limit)}. \tag{12}$$

Equation (12) forms the basis of the perturbation theory developed below.

The inextensibility of the rod Eq. (2) couples transverse and longitudinal coordinates. Resolving it for $r_\parallel'$ and expanding the square root, it reads

$$\rho(s,t) = r_\parallel' = \frac{1}{2}\mathbf{r}_\perp'^2 + O(r_\perp'^4). \tag{13}$$

From Eq. (12), $r_\perp'$ is of order $O(\epsilon^{1/2})$ and the terms neglected in Eq. (13) are of order $O(\epsilon^2)$.

We now turn to the derivation of the equations of motion in terms of $\mathbf{r}_\perp$ and $r_\parallel$. In the case of low Reynolds numbers the dynamics is determined by the balance of elastic, driving, and friction forces. The elastic force derives from

$$\mathcal{H} = \mathcal{H}_0 - \frac{1}{2}\int_0^L ds f \mathbf{r}'^2 \tag{14}$$

via functional differentiation [19]. The Lagrange multiplier function $f(s,t)$ is necessary to preserve the arclength constraint Eq. (2). It can be interpreted as a (negative) local line tension.

For elongated slender bodies like thin rods or stiff polymers, it is well justified to assume a local anisotropic friction force (free-draining limit). The anisotropy is due to the fact that the friction coefficient $\zeta_\perp = 2\zeta_\parallel$ (per unit length) of a stiff rod moving perpendicular to its long axis is twice as large as that for longitudinal motion. It can be taken into account by decomposing the contour velocity $\partial_t \mathbf{r}$ into its components parallel and perpendicular to the local tangent $\mathbf{r}'$ [20]. The force balance can then be written in the form $[\zeta_\parallel \mathbf{r}'\mathbf{r}' + \zeta_\perp(1 - \mathbf{r}'\mathbf{r}')]\cdot\partial_t\mathbf{r} = -\delta\mathcal{H}/\delta\mathbf{r}$. To order ϵ, it takes the form

$$\zeta_\perp \partial_t \mathbf{r}_\perp = -\kappa \mathbf{r}_\perp'''' - (f\mathbf{r}_\perp')' \tag{15a}$$

$$\zeta_\parallel \partial_t r_\parallel - (\zeta_\perp - \zeta_\parallel)\mathbf{r}_\perp' \partial_t \mathbf{r}_\perp = -\kappa r_\parallel'''' + f' - (f r_\parallel')'. \tag{15b}$$

The local anisotropy of the friction generates additional terms of order $O(\epsilon^{3/2})$ that are neglected here. For a freely relaxing rod with given initial conditions, the equations of motion Eqs. (15) have to be solved while respecting the local constraint Eq. (13) and the boundary conditions of zero tension, torque, and force at the ends,

$$f|_{0,L} = \mathbf{r}''|_{0,L} = \mathbf{r}'''|_{0,L} = 0. \tag{16}$$

IV. RELAXATION OF A CONFINED WEAKLY BENDING ROD

A. The leading order in ϵ

In the course of our qualitative discussion in Sec. II we showed that the key problem for understanding the bulk of a relaxing rod is the relaxation of a rod section of length $l \ll L$ confined between two immobile walls, as illustrated in Fig. 2. The weakly bending rod section is supposed to be initially perturbed by small wrinkles of length much smaller than l (excited state). Owing to the undulations, the end-to-end distance r is smaller than l, by an amount $\varrho(t)l$, where

$$\varrho(t) \equiv \frac{1}{l}\int_0^l ds \varrho(s,t) = \frac{r_\parallel(l) - r_\parallel(0)}{l} \tag{17}$$

is the spatial average of the stored length density $\varrho(s,t)$ introduced in Eq. (10). With the help of Eq. (13), we can express $\varrho(t)$ in terms of the transverse displacements,

$$\varrho(t)l = \frac{1}{2}\int_0^l ds \mathbf{r}_\parallel'^2(s,t) + O(\epsilon^2). \tag{18}$$

By exerting a compressing force $f(t)$ on the rod ends, the walls keep the rod section from expanding and the total stored length $\varrho(t)l$ remains constant,

$$\Delta\varrho(t) \equiv \varrho(t) - \varrho^0 = 0, \tag{19}$$

where $\varrho^0 = \varrho(0) = O(\epsilon)$ is the contour length initially stored in the rod section. Our question is, how does such an "excited" rod relax to the ground state, in which the contour has only one buckle of wavelength l (as depicted in Fig. 2).

In the present section we will apply regular perturbation theory to address this problem, i.e., all derivations are understood to hold *to leading order in* ϵ. This allows us to neglect the spatial dependence of the tension. The longitudinal equation of motion Eq. (15b) together with Eq. (12) imply that

$$f' = O(\epsilon). \tag{20}$$

Therefore spatial variations of the tension are small in the limit $\epsilon \ll 1$ and the transverse equation of motion Eq. (15a) is to leading order $O(\epsilon^{1/2})$ given by

$$\zeta_\perp \partial_t \mathbf{r}_\perp = -\kappa \mathbf{r}_\perp'''' - f(t)\mathbf{r}_\perp'', \tag{21}$$

where merely the spatial average

$$f(t) \equiv \frac{1}{l}\int_0^l ds f(s,t) \tag{22}$$

of the force $f(s,t)$ enters. The longitudinal force that the walls exert on the segment equals f up to higher-order corrections. Although Eq. (21) is linear for a given force history, the global constraint of fixed end-to-end distance Eq. (19) makes the tension a functional of the contour $\mathbf{r}_\perp(s,t)$. The resulting problem comprised by Eqs. (19) and (21) is therefore still highly nonlinear and in general not analytically tractable. Progress can be made, however, for generic cases (see footnote 2), as will be shown in the following subsections. We will also present exact numerical solutions in order to illustrate the results.

B. Amplification factor

We analyze the problem in two steps. For a given force history $f(t)$ Eq. (21) is linear in $\mathbf{r}_\perp$. Therefore, we can deter-

mine the stored length as a function of the tension via Eq. (18). The second (in general nontrivial) task is then to invert this relation and to determine the correct force history that obeys Eq. (19), i.e., keeps the end-to-end distance r constant.

We decompose the contour of the "caged" section of length l (Fig. 2) into sine functions,

$$\mathbf{r}_\perp(s,t) = \sqrt{2/l}\sum_n \mathbf{a}_n(t)\sin(q_n s), \tag{23}$$

where $q_n = n\pi/l$ is the wave number corresponding to the nth mode, and for definiteness hinged ends have been assumed for the boundary conditions. (The same boundary conditions have been used in molecular dynamics simulations [11].) Then, from Eq. (18) the stored length can be written as

$$\varrho(t)l = \frac{1}{2}\sum_n q_n^2 \mathbf{a}_n^2 \equiv \sum_n \varrho_n l. \tag{24}$$

The elements $\varrho_n(t)l$ of the last sum can be interpreted as the contour length stored in mode n at time t. We obtain a dynamical equation for $\varrho_n(t)$ by first inserting the Fourier decomposition Eq. (23) into Eq. (21) and then multiplying the resulting equation for the mode amplitudes by $\mathbf{a}_n q_n^2/(2l)$:

$$\partial_\tau \varrho_n = 2[-q_n^4 + \varphi(\tau)q_n^2]\varrho_n. \tag{25}$$

Here we introduced a rescaled tension $\varphi \equiv f/\kappa$ and time $\tau \equiv \kappa t/\zeta_\perp$, which have units of $(\text{length})^{-2}$ and $(\text{length})^4$, respectively. Now, all variables of our problem represent powers of lengths. The dispersion relation Eq. (25) exhibits a stable and an unstable band of modes, separated by the wave number $\sqrt{\varphi(\tau)}$. Modes with larger wave numbers shrink exponentially, whereas the others grow exponentially as a consequence of the competition of the *restoring* bending force (dominating at large wave numbers) and the *driving* force (dominating at small wave numbers). This is formally analogous to spinodal decomposition. In this context Eq. (25) with κ measuring the surface tension and f the curvature of the local free energy at the central maximum is known as the Cahn-Hillard equation [16].

After dividing both sides by ϱ_n, Eq. (25) can immediately be integrated:

$$\varrho_n(\tau) = \varrho_n^0 A(q_n,\tau), \tag{26}$$

with the initial values ϱ_n^0, and an "amplification factor"

$$A(q,\tau) \equiv \exp[2q^2(\Phi(\tau) - q^2\tau)]. \tag{27}$$

By Φ we denote the time integral over the tension

$$\Phi(\tau) \equiv \int_0^\tau d\tilde{\tau}\varphi(\tilde{\tau}). \tag{28}$$

The structure of the function $A(q,t)$ becomes more transparent upon introducing the characteristic wave number $Q(\tau)$ corresponding to the position of its maximum,

$$Q^2(\tau) \equiv \frac{\Phi(\tau)}{2\tau}, \tag{29}$$

which is related to $\varphi(\tau)$ by

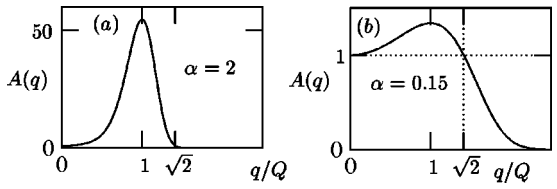

FIG. 4. The sensitive dependence of $A(q,\tau)$, given by Eq. (31b), on the parameter $\alpha = \tau Q^4$. For $\alpha = 2$ the amplification factor takes the form of a pronounced peak (a) whereas for $\alpha = 0.15$ it resembles a step function (b).

$$\varphi = \partial_\tau \Phi = 2\partial_\tau(\tau Q^2). \tag{30}$$

Note that the wave number $Q(\tau)$ that has grown most strongly up to time τ depends on the force history $\varphi(\tilde{\tau} < \tau)$. With this definition, Eq. (27) is rewritten as

$$A(q,\tau) = \exp[2\tau q^2(2Q^2 - q^2)] \tag{31a}$$

$$= \exp\{2\alpha(q/Q)^2[2 - (q/Q)^2]\}, \tag{31b}$$

where we introduced the dimensionless parameter

$$\alpha(\tau) \equiv \tau Q^4(\tau). \tag{32}$$

The amplification factor $A(q,\tau)$ describes how the stored length is rearranged for a given force history. In general wave numbers larger than $\sqrt{2}Q$ are damped ($A < 1$) and wave numbers smaller than $\sqrt{2}Q$ are amplified ($A > 1$). Further, the amplification factor depends very sensitively on the parameter α defined in Eq. (32). For $\alpha \gg 1$ the function $A(q,\tau)$ develops a strong peak around $q = Q$ with a height $e^{2\alpha}$ and a relative width $\Delta Q/Q$ of about[3]

$$\Delta Q/Q = (2\sqrt{\alpha})^{-1}, \tag{33}$$

as shown in Fig. 4(a). Hence, for $\alpha \gg 1$ it can be idealized as $e^{2\alpha}\Delta Q\delta(q-Q)$, whereas for $\alpha < 1$, which is illustrated in Fig. 4(b), the function resembles more the step function $\Theta(\sqrt{2}Q - q)$.

We now turn to the second step of determining the force history $\varphi(\tau)$ that makes the dynamics compatible with the constraint of fixed end-to-end distance Eq. (19). This is achieved by inserting Eqs. (24), (26), and (31a) into Eq. (19),

$$0 = \Delta\varrho(\tau) \tag{34a}$$

$$= \sum_n \varrho_n^0[A(q_n,\tau) - 1] \tag{34b}$$

$$= \sum_n \varrho_n^0(\exp\{2\tau q_n^2[2Q^2(\tau) - q_n^2]\} - 1). \tag{34c}$$

For a given time τ Eq. (34c) is an implicit equation for the characteristic wave number $Q(\tau)$ which by its definition Eq. (29) is related to $\Phi(\tau)$, the time integral over the tension. The

[3]We chose ΔQ somewhat arbitrarily to be twice the standard deviation of the peak. ΔQ^{-1} can be interpreted as a coherence length over which the contour of the rod can be considered to be a pure sinusoidal.

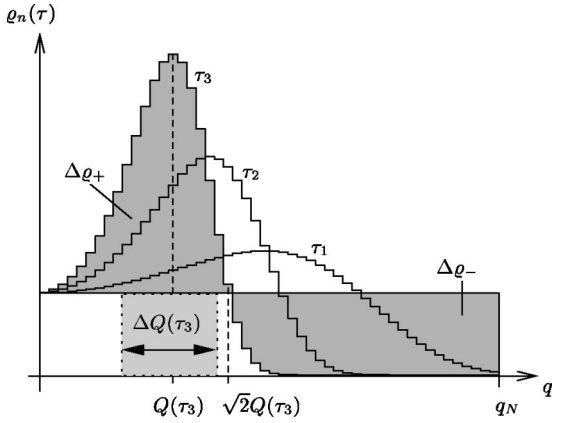

FIG. 5. The fraction $\varrho_n(\tau)=\varrho_n^0 A(q_n,\tau)$ of contour length stored in mode n versus the corresponding wave number $q_n=n\pi/l$ for three successive times $\tau_3>\tau_2>\tau_1$ and the particular initial condition $\varrho^0_{n\leqslant N}=$const and $\varrho^0_{n>N}=0$. The location of the maximum $Q(\tau)$ of $A(q,\tau)$ has been obtained upon solving the implicit equation (34c) numerically. As explained in the main text the dark shaded areas $\Delta\varrho_-$ and $\Delta\varrho_+$ can be interpreted as stored length that has been destroyed and generated during the relaxation, respectively. The global constraint of fixed stored length requires their sum to vanish identically, Eq. (37).

remainder of Sec. IV is devoted to the analysis of the time dependence of the solutions $Q(\tau)$ of Eq. (34c).

First of all, we note that numerically it is straightforward to solve the implicit equation for any initial condition ϱ_n^0. This allows us to illustrate a key feature of the relaxation process right away, namely, the continuous transfer of stored length from small to large scales. Figure 5 shows the mode-number-dependent fraction of stored length $\varrho_n(\tau)$ at three successive times $\tau_1<\tau_2<\tau_3$ for the initial condition $\varrho^0_{n\leqslant N}=\varrho^0/N=$const and $\varrho^0_{n>N}=0$. For this particular choice of initial conditions $\varrho_n(\tau)$ can up to a constant prefactor be identified with $A(q_n,\tau)$. The dark gray area represents the difference between the stored lengths at times 0 and time τ_3. It has two natural subdivisions $\Delta\varrho_+>0$ and $\Delta\varrho_-<0$, adding up to zero by virtue of the constraint Eq. (34b). Formally, we define by

$$\Delta\varrho_-(\tau)\equiv\sum_{n=N_c}^{\infty}\varrho_n^0[A(q_n,\tau)-1]<0, \tag{35}$$

with N_c being the smallest n with $q_n>\sqrt{2}Q(\tau)$, the stored length that has been "destroyed" up to time τ. Note that each element of the sum Eq. (35) is negative. Similarly, $\Delta\varrho_+(\tau)$ represents the stored length that has been "generated" in the modes with wave numbers below $\sqrt{2}Q(\tau)$, i.e., we define

$$\Delta\varrho_+(\tau)\equiv\sum_{n=0}^{N_c-1}\varrho_n^0[A(q_n,\tau)-1]>0. \tag{36}$$

Since the total change in stored length $\Delta\varrho$ must vanish,

$$\Delta\varrho(\tau)\equiv\Delta\varrho_+(\tau)+\Delta\varrho_-(\tau)=0, \tag{37}$$

we can imagine the relaxation process as a *transfer* of stored length $|\Delta\varrho_-(\tau)|$ from scales smaller than $(\sqrt{2}Q)^{-1}$ to scales larger than $(\sqrt{2}Q)^{-1}$ in time τ. Due to the form of the amplification function (see Fig. 4) the mode amplitudes with wave number close to $Q(\tau)$ show the largest increase up to time τ. In the present case this results in the formation of a pronounced peak around $Q(\tau_3)$ although the initial excitation was "flat" up to the cutoff.

It will turn out in the next section that a large peak in the amplification factor implies power-law evolution of the characteristic wave number $Q(\tau)$ and thus of the tension $\varphi(\tau)$. Whether or not the mode spectrum develops a pronounced peak as in the above example depends on the initial conditions. Figure 5 suggests that a strong peak is present at time τ_3, because the dark gray areas $\Delta\varrho_+$, $-\Delta\varrho_-$ are much larger then the light gray area. In other words, the stored length will be strongly localized around $Q(\tau)$ at time τ, if the relaxed stored length $|\Delta\varrho_-|=\Delta\varrho_+$ is much larger than the contour length that was initially stored in the interval of width ΔQ around the wave number Q. To estimate the former, we first note that $A(q,\tau)$ decays exponentially to zero for $q>\sqrt{2}Q$, so that we simply replace it by zero in Eq. (35). Then, because many modes contribute to the remaining sum, we take the continuum limit in mode space according to

$$\varrho^0(q=q_n)\equiv\frac{\varrho_n^0}{\pi/l}, \tag{38}$$

so that we obtain

$$\Delta\varrho_-\approx-\int_{\sqrt{2}Q}^{\infty}dq\varrho^0(q). \tag{39}$$

The amount of contour length initially stored around Q can be estimated by the initial amplitude at Q, $\varrho^0(Q)$, multiplied by the width of the peak ΔQ. Upon comparing $\varrho^0(Q)\Delta Q$ with $\Delta\varrho_-$ we obtain the criterion

$$\int_{\sqrt{2}Q}^{\infty}dq\varrho^0(q)\gg\varrho^0(Q)\Delta Q\Leftrightarrow\text{peak in }A(q,\tau), \tag{40}$$

to decide whether a peak is expected for a given value of $Q(\tau)$.

Assuming condition Eq. (40) to hold, we will show in the next section how *approximate* power-law relaxation of the dominant wave number $Q(\tau)$ and of the tension $\varphi(\tau)$ emerges. In Sec. IV D we will see that *exact* power-law solutions of Eq. (34c) moreover arise from self-affine initial conditions $\varrho^0(q)\propto q^{-\beta}$ with $1<\beta<3$. It will turn out that a complete classification of all generic (see footnote 2) relaxation scenarios in the bulk can be given in terms of the exponent β, characterizing the roughness of the initial contour.

C. Cascading of stored length

Provided that the condition Eq. (40) is satisfied at a time τ larger than some suitable short transient time, the relaxation has accumulated most of the stored length ϱ^0 in the peak around $Q(\tau)$. Undulations of wavelength Q^{-1} visibly dominate the rod contour. Furthermore, the sum Eq. (36) representing $\Delta\varrho_+$ is dominated by the modes around $Q(\tau)$, which simplifies its evaluation significantly. Yet, one still has to discriminate two limiting cases.

1. Intermediate asymptotics

The peak of the amplification factor covers many modes, i.e., the width ΔQ of the amplification peak, as defined in Eq. (33), is much larger than the mode spacing π/l, or

$$Ql \gg 2\pi\sqrt{\alpha}. \tag{41}$$

Then many modes contribute to both, $\Delta\varrho_-$ and $\Delta\varrho_+$ and the corresponding sums Eqs. (35) and (36) can be converted into integrals, as has already been done in Eq. (39) for $\Delta\varrho_-$ to obtain the criterion Eq. (40). The continuum limit for $\Delta\varrho_+$ reads

$$\Delta\varrho_+ \approx \int_0^{\sqrt{2}Q} dq\varrho^0(q)\{\exp[2\tau q^2(2Q^2-q^2)]-1\}. \tag{42}$$

Since by assumption, Eq. (40), the integrand in Eq. (42) has a pronounced maximum, it can be evaluated by a saddle point approximation, replacing it effectively by the area $\Delta Q \exp(2\alpha)$ under the amplification peak $A(q)$ multiplied by $\varrho^0(Q)$,

$$\Delta\varrho_+ \approx \varrho^0(Q)\Delta Q \exp(2\alpha). \tag{43}$$

The conservation of the stored length, Eq. (37), implies

$$0 = \Delta\varrho(\tau) \approx \varrho^0(Q)\Delta Q \exp(2\alpha) - \int_{\sqrt{2}Q}^{\infty} dq\varrho^0(q). \tag{44}$$

Since the first term on the right-hand side of Eq. (44) depends exponentially on the parameter α, the latter is slaved to be time independent up to logarithmic corrections,

$$\alpha = \text{const} + O(\ln\tau). \tag{45}$$

Recalling the definition of α, Eqs. (32), and using Eq. (30), one finds for the tension

$$\varphi(\tau) = Q(\tau)^2 \propto \tau^{-1/2}, \tag{46}$$

which proves Eqs. (4) and (6) up to logarithmic corrections for the intermediate asymptotics emerging once Eq. (40) is satisfied. While the peak position is thus migrating to lower wave numbers according to the power law $Q(\tau)\propto\tau^{-1/4}$, its width shrinks accordingly, $\Delta Q\propto\tau^{-1/4}$. Consequently, the number of discrete modes under the amplification peak decreases.

2. Ultimate staircase relaxation

When ΔQ eventually becomes smaller than the mode spacing π/l, the contour of the rod starts to be dominated by the discrete wave number $q_{n^\star}$ closest to $Q(\tau)$. Thus it is no longer legitimate to approximate $\Delta\varrho_+$ by an integral. On the contrary, in the limit

$$Ql \ll 2\pi\sqrt{\alpha} \tag{47}$$

the sum in Eq. (36) should be replaced by the single dominant element corresponding to the index $n^\star$,

$$\Delta\varrho_+ = \varrho^0_{n^\star}\exp[2\tau q_{n^\star}(2Q^2-q_{n^\star}^2)]. \tag{48}$$

In contrast, the sum $\Delta\varrho_-$ representing the destroyed stored length has contributions from many modes even in the limit

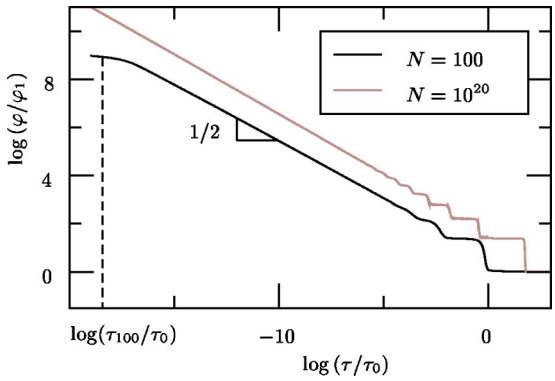

FIG. 6. Typical tension relaxation of a rod with initial conditions satisfying Eq. (40) from a numerical solution of Eq. (34c). As in the example of Fig. 5 we chose the particular initial condition $\varrho^0_{n\leqslant N}$ = const and $\varrho^0_{n>N}=0$. For two values of N the graph displays the tension φ versus time τ in units of critical force $\varphi_1=(\pi/l)^2$ and the typical relaxation time $\tau_0=l^4$, respectively. In the case $N=100$ it is seen that the intermediate asymptotic power law $\varphi\propto\tau^{1/2}$ is valid in the time window $\tau_N\ll\tau\ll\tau_0$, where $\tau_N\equiv N^{-4}\tau_0$ is the relaxation time of the highest excited mode. The extreme case $N=10^{20}$ illustrates the asymptotic behavior of the staircase regime for large N.

Eq. (47) and it can still be approximated by the integral Eq. (39). The parity of created and destroyed stored lengths, Eq. (37), now takes the form

$$\varrho^0_{n^\star}\exp[2\tau q_{n^\star}(2Q^2-q_{n^\star}^2)] \approx \int_{\sqrt{2}Q}^{\infty} dq\varrho^0(q). \tag{49}$$

As below Eq. (44) we conclude that the exponent on the left-hand side has to stay constant in time up to logarithmic contributions. By using the definition of Q, Eq. (29), this implies that the tension is equal to the Euler force corresponding to the mode $n^\star$,

$$\varphi \approx q_{n^\star}^2, \tag{50}$$

as long as $n^\star$ is indeed the dominant mode. In fact, the discrete $n^\star$ is a time-dependent quantity that evolves in steps and approaches 1 in the final stage of the relaxation, which corresponds to the first Euler buckling mode.

To illustrate the above discussion, Fig. 6 displays the (normalized) line tension $\varphi(\tau)$ obtained from the numerical solution of the implicit Eq. (34c) for $Q(\tau)$. The relaxation scenario shown is characteristic of the dynamics for the class of initial conditions satisfying the condition in Eq. (40). For short times, one observes after a short transient period a smooth intermediate asymptotic power-law behavior $\varphi(\tau)\sim\tau^{-1/2}$, which for long times develops staircaselike oscillations with plateaus at $\varphi_n=n^2\varphi_1(n\in\mathbb{N})$, in agreement with the above derivation.

D. Exact similarity solutions

In addition to the cascading of stored length that is strongly localized in mode space, there is a different mechanism giving rise to the power law Eq. (4). This is revealed by explicitly searching for similarity solutions of Eq. (34c) un-

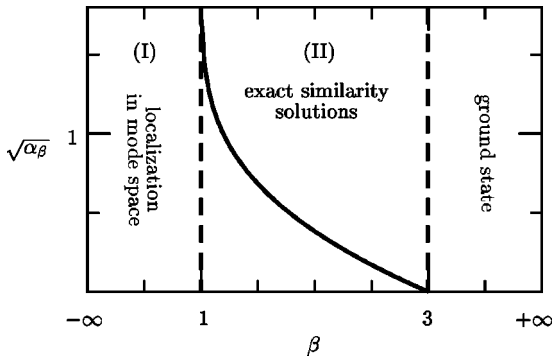

FIG. 7. The amplitude $\sqrt{\alpha_\beta}$ in the power law Eq. (53) for the line tension φ in the bulk of a relaxing rod with power-law initial conditions $\varrho^0(q) \propto q^{-\beta}$. For $\beta<1$ (type I initial conditions) an upper cutoff is required to keep the stored length finite. The relaxation then proceeds via the cascading of a localized peak in mode space, as depicted in Fig. 4(a) and explained in Sec. IV C. For $\beta>3$, the rod is essentially in the ground state from the beginning. The interval $1<\beta<3$ of type II initial conditions comprises the exact similarity solutions derived in Sec. IV D. Thermal initial conditions correspond to $\alpha_{\beta=2} \approx 0.146$.

der the condition that many modes contribute to the relaxation dynamics and the sums in Eq. (34c) can again be converted into integrals. In contrast to the intermediate asymptotic power-law solutions obtained in Sec. IV C, which obeyed $\alpha=$const only up to logarithmic corrections, solutions $Q(\tau)$ of the continuum limit of the constraint Eq. (34c),

$$0 = \int_{l^{-1}}^{\infty} dq \varrho^0(q) \{\exp[2\tau q^2(2Q^2 - q^2)] - 1\}, \tag{51}$$

can be found that *exactly* obey

$$\alpha \equiv Q^4 \tau \stackrel{!}{=} \text{const}. \tag{52}$$

Inserting the ansatz

$$\varphi(\tau) = Q^2(\tau) = (\alpha/\tau)^{1/2} \tag{53}$$

with a yet undetermined time-independent parameter α into Eq. (51) and changing variables $q \to q(\alpha/\tau)^{1/4}$, we obtain

$$0 = \int_{\tau^{1/4}/l\alpha^{1/4}}^{\infty} dq \varrho^0\left(\frac{q\alpha^{1/4}}{\tau^{1/4}}\right) \{\exp[2\alpha(-q^4 + 2q^2)] - 1\}. \tag{54}$$

This is mathematically equivalent to Eq. (34c) as long as the integral is not sensitive to its (small) lower bound, so that the latter can effectively be taken to be zero. Then, for the integral to be independent of time, the initial condition has to be of the power-law form,

$$\varrho^0(q) = \Lambda^{1-\beta} q^{-\beta}, \tag{55}$$

where the length Λ has to be introduced on dimensional grounds. The numerical solutions $\alpha=\alpha_\beta$ of Eq. (54) are depicted in Fig. 7 as a function of β. As can be seen, the roughness exponent β is not completely arbitrary. In fact, no finite solutions for α exist outside the interval $1<\beta<3$.

For $1<\beta<3$, the ansatz Eq. (55) solves Eq. (54) exactly in the limit that the lower bound tends to zero, or for times

$$\tau \ll \alpha_\beta l^4. \tag{56}$$

Then the initial conditions Eq. (55) parametrize a class of power-law solutions (to our knowledge) not seen previously. The algebraic decay law can in this case be attributed to the self-affine geometry of the initial conformation. Note that the weakly bending condition expressed in Eqs. (12) and (11) requires

$$\varrho^0 \approx \int_{l^{-1}}^{\infty} dq \varrho^0(q) = \frac{(l/\Lambda)^{\beta-1}}{\beta - 1} \ll 1, \tag{57}$$

i.e., $\Lambda \gg l$ for a rod section of length l. An important example of these initial conditions is provided by the contour of a stiff polymer in thermal equilibrium ($\beta=2$) [13,14], for which the length $2\Lambda/\pi$ is identified as the persistence length of the polymer, which indeed has to be much larger then the length of the polymer in the weakly bending limit. The corresponding amplification factor $A(q)$ with $\alpha_{\beta=2} \approx 0.146$ as a function of q is shown in Fig. 4(b).

In contrast to the intermediate asymptotics discussed in Sec. IV C, the dynamics for power-law initial conditions with $1<\beta<3$ is not necessarily governed by a characteristic wave number that visibly dominates the contour undulations. For $\alpha_\beta \lesssim 1$ the amplification factor rather acts as a time-dependent low-pass filter cutting off the mode amplitudes with wave numbers larger than $\sqrt{2}Q(\tau)$. This is to be contrasted with the situation in Fig. 4(a), where the amplification factor is strongly peaked around $Q(\tau)$. Only in the limit $\beta \to 1$ do the self-affine initial conditions Eq. (55) satisfy the condition Eq. (40) that guarantees a large peak in the amplification factor, thus giving way to the scenario described in Sec. IV C, but *without* logarithmic corrections.

E. Classification of power-law initial conditions

The fact that the value $\alpha=\alpha_\beta$ that solves Eq. (54) diverges as β approaches 1 from above indicates an unphysical situation. The initially stored length in modes with large wave numbers grows without bound and the integral over $\varrho^0(q)$ diverges. Hence for $\beta \lesssim 1$ power-law initial conditions as in Eq. (55) are well defined only with an upper cutoff, say, the wave number q_N corresponding to the highest excited mode with index N. Furthermore, with Eq. (55) the weakly bending condition now requires $q_N \Lambda \ll 1$. Then, for times τ such that $Q(\tau) \ll q_N$, the initial conditions automatically satisfy the criterion Eq. (40). Hence, after a transient time, power-law initial conditions with exponents $\beta \lesssim 1$ relax according to the cascading scenario of Sec. IV C characterized by localization in mode space.

We thus observe that the two distinct bulk-relaxation scenarios described in Secs. IV C and IV D are characteristic of power-law initial conditions with $\beta<1$ and $1<\beta<3$, respectively. This suggests a classification of the typical relaxation dynamics according to the exponent β. Accordingly, we classify initial conditions of the power-law form in Eq. (55) as type I if $\beta<1$ and as type II if $1<\beta<3$. Further

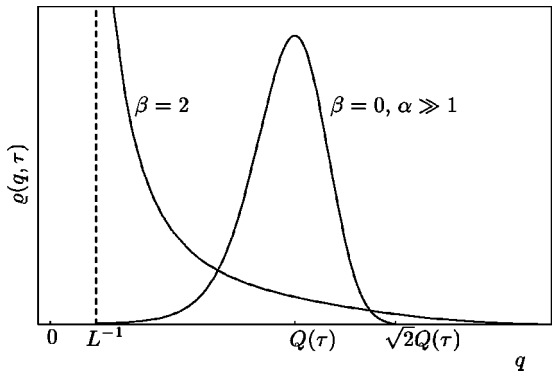

FIG. 8. The situation in mode space after time τ for representative initial conditions of type I ($\beta=0$, $\alpha\gg1$, cutoff $q_N\gg Q$ as in Fig. 5) and type II (thermal initial conditions $\beta=2$) with the same total stored length ϱ^0.

support for the pertinence of this distinction will emerge in the following. Both the conformational relaxation (see the following paragraph) and the boundary relaxation (see Sec. V) will be seen to be markedly different for type I and type II initial conditions.

The case $\beta>3$ can be dismissed for the following reason. Upon expanding the integrand of Eq. (54) into a Taylor series for small q, it is seen that for $\beta>3$ the integral would be dominated by the lower bound, indicating the breakdown of the continuum approximation. The sum in Eq. (34c) is then dominated by its first term, the first Euler buckling mode. This yields a tension of about $\varphi\approx\varphi_1\propto l^{-2}$: A confined buckled rod with the initial condition Eq. (55) and $\beta>3$ is essentially in the ground state from the beginning.

We have thus achieved a complete classification of the possible relaxation scenarios for all generic initial conditions (see footnote 2) for the key problem of a longitudinally confined rod, which was previously studied in numerical simulations [11]. The results are summarized in Fig. 7. The power-law decay Eq. (4) of the tension emerges as a quite universal feature of the problem, whereas the accompanying conformational relaxation will now be shown to be fundamentally different for type I and type II initial conditions.

F. Conformational relaxation

For type I initial conditions the intermediate asymptotic dynamics is completely governed by the characteristic wavelength Q^{-1}. The latter directly determines the tension and visibly dominates the real-space image of the contour, so that tension decay and conformational relaxation proceed hand in hand. A markedly different scenario results for type II initial conditions. To appreciate the difference, consider the representative distributions of stored length in mode space for type I and type II initial conditions as they have evolved after time τ (Fig. 8). The stored length that was initially distributed in the tails $q\geqslant\sqrt{2}Q(\tau)$ has been accumulated around $Q(\tau)$. Due to the substantially different relative weight of these tails in the initial conditions, the corresponding distributions at time τ look utterly different. While over a time interval 16τ the undulations dominating the real space image of the contour will have doubled their wavelength under type I conditions, the corresponding evolution of $Q(\tau)$ will have hardly any noticeable consequences on the real-space image of a type II contour, which is dominated by undulations of much longer wavelengths that are practically stationary on this time scale.

As we pointed out in the Introduction, the relaxation of a laterally confined rod that was discussed in the present section can also be considered an idealization of the situation in the bulk of a long stiff rod with *free* ends that was initially under high pressure, which also has been simulated [12]. At the free ends, the tension $\varphi(s,\tau)$ has to vanish as a consequence of the boundary conditions Eq. (16). In the following we face the question of how it falls off between the bulk and the ends.

V. THE RELAXATION FOR OPEN BOUNDARIES

In the present section and in the Appendix, we develop a method to treat situations where the tension exhibits substantial spatial variations along the rod. The basic idea is as follows. The major variation of the tension, namely, from its bulk value to zero at the open boundaries, occurs within a (time-dependent) boundary layer of a yet unknown length $\lambda(\tau)$. In the following paragraph we will motivate the crucial length scale separation between $\lambda(\tau)$ and $Q^{-1}(\tau)$. It will allow us to apply our leading order results from Sec. IV *locally* on an intermediate scale $l(\tau)$ ($Q^{-1}\ll l\ll\lambda$), over which the tension does not change appreciably. This in turn will enable us to derive closed equations for a suitably coarse-grained tension profile $\varphi_l(s,\tau)$ in Sec. V B. This adiabatic approximation will eventually be justified by a consistency check. (Its precise relation to the regular perturbation scheme of Sec. IV will be clarified at the end of Sec. V and in the Appendix.) Our discussion of the boundary-layer problem will parallel the discussion in Sec. IV in discerning again type I and type II initial conditions. Thereby we will in particular recover for the bulk our earlier results, which were based on the assumption of longitudinal confinement.

A. Length scale separation

Technically, to address spatial variations in the tension profile, which could be discarded as of higher order in ϵ in the regular perturbation scheme of Sec. IV A, we need to push the analysis beyond the leading order. In Sec. IV B we have determined the time evolution of the transverse displacements $\mathbf{r}_\perp(s,\tau)$ of a rod section of length l to leading order in ϵ. By inserting with the help of Eq. (13) the result back into the (higher-order) equation of motion Eq. (15b) for $\mathbf{r}_\parallel$, we can iteratively estimate the order of magnitude of the spatial variation of the tension, which is determined by the nonlinear terms.

Note that the leading-order solution for $\mathbf{r}_\perp(s,\tau)$ depends on the force history of the particular rod section under consideration, which enters via the characteristic wave number $Q(\tau)$. We recall from our discussion of the amplification factor in Sec. IV B that $\sqrt{2}Q(\tau)$ acts as an effective ultraviolet

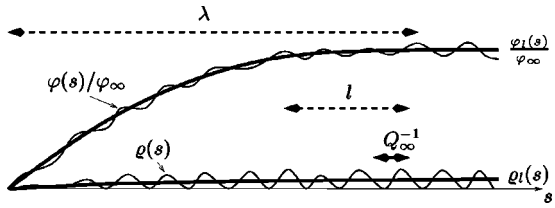

FIG. 9. The length λ over which the tension increases toward the bulk value is much larger than the characteristic length Q_∞^{-1} of the transverse undulations in the bulk, as expressed by the inequality in Eq. (60). The slowly varying part $\varphi_l(s)$ of the tension is obtained upon averaging over the coarse-graining scale l that satisfies the condition in Eq. (61).

cutoff for the contour undulations. From Eqs. (13) and (12), we thus have for example

$$2r_\parallel'''' = (\mathbf{r}_\perp'^2)''' \leqslant Q^3 O(\epsilon). \tag{58}$$

Time derivatives are estimated by recourse to Eq. (15a). Applying this reasoning to Eq. (15b) after differentiating with respect to arclength s, one eventually finds

$$\varphi'' \leqslant Q^4 O(\epsilon) \tag{59}$$

for the order of magnitude of the tension variations. Generalizing $Q(\tau) \to Q(s,\tau)$ to allow for a slow spatial variation of the characteristic wavelength, we can integrate Eq. (59) from one end of the contour, where $\varphi = 0$ and $Q = 0$, toward the bulk, where $\varphi \equiv \varphi_\infty = Q^2 \equiv Q_\infty^2$. (Here and in the following, we symbolically write "∞" to refer to regions deep in the bulk.) Since $Q \leqslant Q_\infty$, we can infer

$$Q_\infty^2 = \varphi_\infty = \int_0^\lambda ds \int_0^s d\hat{s}\varphi'' \leqslant Q_\infty^4 \lambda^2 O(\epsilon)$$

by integrating through the boundary layer of length $\lambda(\tau)$. From this we read off a lower bound for the order of magnitude of λ,

$$\Rightarrow (\lambda Q_\infty)^{-1} \leqslant O(\epsilon^{1/2}). \tag{60}$$

For small $\epsilon \to 0$, we thus have a strong length scale separation between the wavelength Q_∞^{-1} of the dynamically most active contour undulations and the scale λ of the substantial tension variations, i.e., $\lambda \gg Q_\infty^{-1}$. It allows us to define a length $l(t)$ intermediate between the characteristic scales $Q_\infty^{-1}(t)$ and $\lambda(t)$, so that

$$1 \ll Q_\infty l \ll \epsilon^{-1/2}. \tag{61}$$

Figure 9 illustrates the relation between the various lengths. An immediate consequence of the inequalities Eqs. (60) and (61) is that we can imagine the free rod at any time as consisting of rod sections of length $l \gg Q_\infty^{-1}$, each of which is subject to a uniform "average" tension. After specifying this average we will be ready to *locally* apply our results of Sec. IV to the problem of a rod with free ends in the next sections.

B. Adiabatic approximation

The length scale separation observed in the previous section suggests to look for a mathematical description of the "substantial" variation of the tension on the scale λ without its complicated wiggling on the "microscale" Q_∞^{-1}, which is at most of order $Q_\infty^2 O(\epsilon)$. The natural way to get rid of the short-wavelength fluctuations without losing the substantial part is to consider coarse-grained quantities that are averaged over the intermediate scale l. More precisely, we define for any arclength-dependent quantity $g(s)$ a corresponding coarse-grained quantity $g_l(s)$ by

$$g_l(s) \equiv \frac{1}{l}\int_{-l/2}^{l/2} d\sigma g(s+\sigma). \tag{62}$$

It will turn out that for the quantities of interest this average is actually *independent* of l to leading order in ϵ, if l obeys the double inequality Eq. (61). For the tension $\varphi(s,\tau)$ this was already established in Sec. V A.

A closed equation for the coarse-grained tension φ_l can now be derived from the full equations of motion, Eqs. (15). Upon integrating the longitudinal Eq. (15b) with respect to the arclength and using the free boundary conditions Eq. (16), we at first obtain an explicit equation for the spatially varying tension $\varphi(s,\tau)$ before coarse-graining,

$$\varphi(s,\tau) = \hat{\zeta}\int_0^s d\tilde{s}\partial_\tau r_\parallel - (1-\hat{\zeta})\int_0^s d\tilde{s}\mathbf{r}_\perp'\partial_\tau \mathbf{r}_\perp + r_\parallel'''(s) + \varphi(s,\tau)r_\parallel'(s). \tag{63}$$

Here $\hat{\zeta} = \zeta_\parallel/\zeta_\perp = 1/2$ is the ratio between the transverse and longitudinal friction coefficients. Using our knowledge about the bulk we now show that only the first term on the right hand side is able to produce a term of the order of the tension φ_∞ in the bulk. Counting arclength derivatives in orders of Q_∞ in the spirit of Sec. V A, φ_∞ is estimated as of order $O(Q_\infty^2)$. The crucial fact that $\sqrt{2}Q_\infty$ acts as a high-wavenumber cutoff for the contour fluctuations together with the local constraint Eq. (13) implies that the last two terms are $O(\epsilon Q_\infty^2)$ and thus always small compared to the bulk tension φ_∞. The same reasoning can be applied to the second term on the right-hand side after suitable partial integrations,

$$\left|\int_0^s d\tilde{s}\mathbf{r}_\perp'\partial_\tau\mathbf{r}_\perp\right| \overset{\text{Eq. (15a)}}{=} \left|\int_0^s d\tilde{s}\mathbf{r}_\perp'(-\mathbf{r}_\perp'''' - (\varphi\mathbf{r}_\perp')')\right| \overset{\varphi<\varphi_\infty}{\leqslant} |\mathbf{r}_\perp'\mathbf{r}_\perp'''| + \mathbf{r}_\perp''^2 + \varphi_\infty\mathbf{r}_\perp'^2 = O(\epsilon Q_\infty^2).$$

Consequently, the necessary $O(Q_\infty^2)$ term on the right-hand side of Eq. (63) must be the one depending on the longitudinal velocity $\partial_\tau r_\parallel$. It represents the pressure that is generated in the rod by the outward motion of the relaxing boundary layer. Differentiating Eq. (63) twice with respect to arclength and integrating over time we can therefore write to leading order

$$\hat{\zeta}^{-1}\Phi'' = \hat{\zeta}^{-1}\int_0^\tau d\hat{\tau}\varphi''(s,\hat{\tau}) = \varrho(s,\tau) - \varrho(s,0). \tag{64}$$

Since we are interested in the long-wavelength fluctuations of φ, we average this equation over the length l and obtain

$$\hat{\zeta}^{-1}\Phi_l''(s,\tau) = \Delta\varrho_l(s,\tau). \tag{65}$$

The physical interpretation of this important result is that the release $\Delta\varrho_l \equiv \varrho_l(s,\tau) - \varrho_l(s,0) < 0$ of stored length corresponds to a negative curvature in the time integrated tension profile $\Phi_l'' < 0$. Stored-length release acts as a source for spatial variations of the time integrated tension. For increasing arclength s we expect the tension to saturate, $\Phi''(s\to\infty) \to 0$, corresponding to a conserved stored length in the bulk, $\Delta\varrho_l(s\to\infty) = 0$, just as we argued throughout Sec. IV. In this sense, Eq. (65) generalizes the conservation law Eq. (19) for the bulk to the boundary layer. For the interested reader a second, more formal derivation of Eq. (65) via the method of multiple scales [21] is given in the Appendix.

In order to close Eq. (65) we need an expression for the stored-length release $\Delta\varrho_l$ on the scale l as a function of Φ_l. Here, we can simply refer back to Sec. IV B. There we have dealt with one "coarse-graining element" of length l to leading order in ϵ. We recall that a crucial ingredient of the (ordinary) perturbation calculation in Sec. IV B was that we could neglect spatial variations of $\varphi(s,\tau)$ to leading order in ϵ. The length scale separation observed in Sec. V A shows that we can neglect them on the scale l, which is much larger than the characteristic wavelength Q^{-1} of the dynamically most active transverse modes. Therefore, our above perturbative results can be used in the present boundary layer calculations. With the Eqs. (26)–(30) and (31a) we can describe the evolution of $\varrho_l(s,\tau)$ as a function of $\varphi_l(s,\tau)$ by identifying the coarse-grained quantities with the corresponding spatial averages in Eqs. (17) and (22). This identification constitutes the adiabatic approximation.

The stored-length release in the continuum limit is now taken over from the right-hand side of Eq. (51),

$$\Delta\varrho_l(s,\tau) = \int_{l^{-1}}^{\infty} dq\varrho^0(q)[e^{2\pi q^2[2Q_l(s,\tau)^2 - q^2]} - 1] \tag{66}$$

with $Q_l(s,\tau)$ the spatially weakly varying, adiabatic quantity. There are two things to remark about Eq. (66). First, the use of an integral instead of a sum is legitimate, if the integral is not dominated by its lower bound. We infer from the length scale separation Eq. (61) that this is the case if the integrand is dominated by wave numbers close to the effective upper cutoff $\sqrt{2}Q_l$. The wiggles on the scale Q^{-1} are then the major source for the release of stored length. Second, in the most general case, we should allow for a weak spatial dependence not only of Q_l but of $\varrho^0(q)$ as well by writing $\varrho^0(q,s)$. For simplicity, we neglect such a spatial dependence in the initial conditions and focus on statistically *uniform* initial excitations.

Upon inserting Eq. (66) into Eq. (65) and inferring $Q_l^2(s,\tau) \equiv \Phi_l(s,\tau)/2\tau$ from Eq. (29), we obtain a closed differential equation for Φ_l:

$$\Phi_l''(s,\tau) = \hat{\zeta}\int_{l^{-1}}^{\infty} dq\varrho^0(q)[e^{2q^2[\Phi_l(s,\tau) - q^2\tau]} - 1]. \tag{67}$$

Specializing to the left end of a semi-infinite rod, this equation has to be solved for the boundary conditions $\Phi_l = 0$ (no force) at the end and $\Phi_l'' = 0$ at $s\to\infty$ (conserved stored length in the bulk).

The differential equation (67) is of a type frequently encountered in classical mechanics: By interpreting Φ_l as the position of a particle (mass $\equiv 1$) and s as the time variable, Eq. (67) represents Newton's equation,

$$\Phi_l''(s) = -\partial_{\Phi_l} U(\Phi_l), \tag{68}$$

for a particle moving in a potential $U(\Phi_l)$,

$$U(\Phi_l) = \hat{\zeta}\int_{l^{-1}}^{\infty} dq\varrho^0(q)\left[\Phi_l - \frac{e^{2q^2\Phi_l} - 1}{2q^2}e^{-2q^4\tau}\right]. \tag{69}$$

For fixed time τ, this potential is $\cap$ shaped as a function of Φ_l. The mechanical analog to our task is to find the instanton solution ϕ_l, which approaches the location of the maximum of $U(\phi_l)$ as $s\to\infty$. Equation (68) can be integrated numerically for all times and arbitrary initial conditions $\varrho^0(q)$. Having obtained $\Phi_l(s,\tau)$, the tension profile $\varphi(s,\tau)$ is extracted by taking the derivative

$$\varphi_l(s,\tau) = \partial_\tau \Phi_l(s,\tau). \tag{70}$$

Analytical progress is again possible for the generic relaxation scenarios that emerged from the discussion of the bulk in Sec. IV. We therefore take the initial conditions to be of the power-law form in Eq. (55). To simplify the notation we will from now on drop the subscripts "l" for coarse-grained quantities. As before, we consider type I and type II conditions separately.

C. Exact similarity solutions

For type II initial conditions, i.e., Eq. (55) with $1 < \beta < 3$, one can find exact similarity solutions of Eq. (67). To this end, we make the dynamic scaling ansatz

$$\Phi(s,\tau) = \tau^{1/2}\psi_\beta\left(\frac{s}{\lambda_\beta(\tau)}\right) \tag{71}$$

for the integrated force, with the characteristic length

$$\lambda_\beta(\tau) = \hat{\zeta}^{-1/2}\Lambda^{1-4\delta_\beta}\tau^{\delta_\beta} \quad \text{and} \quad \delta_\beta = \frac{3-\beta}{8}. \tag{72}$$

In Eq. (71) the bulk dynamics has been explicitly taken out of the scaling form, and the definition of λ_β naturally results from inserting Eq. (71) into Eq. (67) with the aim of eliminating the parameter dependence. That the resulting differential equation for $\psi_\beta(\xi)$ is in particular time independent for $\tau \ll l^4$ is more easily seen after another variable transformation $q \to \tilde{q}\tau^{-1/4}$,

$$\psi_\beta''(\xi) = \int_{\tau^{1/4}/l}^{\infty} d\tilde{q}\tilde{q}^{\,-\beta}[e^{2\tilde{q}^2[-\tilde{q}^2 + \psi_\beta(\xi)]} - 1]. \tag{73}$$

The boundary conditions are $\psi_\beta(0) = \psi_\beta'(\xi\to\infty) = 0$. Having solved Eq. (73) for $\psi_\beta(\xi)$, the tension is extracted by differentiation,

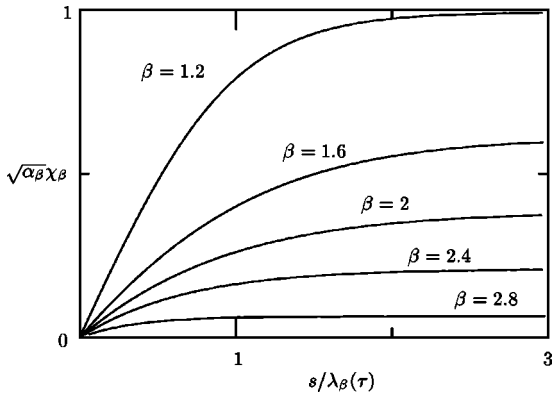

FIG. 10. Type II: Stress profile in the boundary layer, given by the scaling function $\chi_\beta(s/\lambda_\beta(\tau))$, Eq. (74). The case $\beta=2$ corresponds to thermalized initial conditions.

$$\varphi(s,\tau) = \partial_\tau \Phi_l(s,\tau) = \partial_\tau \left[\tau^{1/2} \psi_\beta\left(\frac{s}{\lambda_\beta(\tau)}\right)\right] \equiv \sqrt{\frac{\alpha_\beta}{\tau}}\chi_\beta\left(\frac{s}{\lambda_\beta}\right). \tag{74}$$

To make contact with Eq. (53), the amplitude $\sqrt{\alpha_\beta}$ calculated in Sec. IV D (see Fig. 7) was explicitly taken out of the scaling function, so that the latter is normalized, $\chi(\xi\to\infty)=1$. The combination $\sqrt{\alpha_\beta}\chi_\beta(\xi)$ then obeys

$$\sqrt{\alpha_\beta}\chi_\beta(\xi) = \frac{1}{2}\psi_\beta(\xi) - \frac{3-\beta}{8}\xi\psi'_\beta(\xi). \tag{75}$$

In Fig. 10 the numerical solutions are shown for different values of β. We have plotted the combination $\sqrt{\alpha_\beta}\chi_\beta(s/\lambda_\beta)$ instead of the normalized scaling function χ_β, because the graphs of the latter cross each other for different β, rendering the figure too crowded. The slope $\chi'_\beta(\xi)$ at the origin thus has a somewhat weaker dependence on β as suggested by Fig. 10. It is seen that $\chi_\beta(s/\lambda_\beta)$ saturates for $s\simeq\lambda_\beta$, which establishes λ_β as the characteristic width of the boundary layer. Figure 10 moreover shows that the tension profiles have a nonzero curvature throughout the boundary layer. According to Eq. (65) the release of tension and stored length is thus spread over the whole boundary layer. Observe that $\Lambda^{1-4\delta_\beta} \propto 1/\sqrt{\varrho^0}$ from Eq. (57) so that

$$\lambda_\beta \propto \tau^{\delta_\beta}/\sqrt{\varrho^0}. \tag{76}$$

Interestingly, the small parameter $\sqrt{\varrho^0}=O(\epsilon^{1/2})$ appears in the denominator so that the limits $\tau\to 0$ and $\epsilon\to 0$ do not interchange. This indicates that the boundary-layer phenomena are not accessible by ordinary perturbation theory in ϵ.

In the interesting case of thermal initial conditions ($\beta=2$) the boundary layer $\lambda_{\beta=2}(\tau)$ grows according to

$$\lambda_2(\tau) = \hat{\zeta}^{-1/2}\Lambda^{-1/2}\tau^{1/8}, \tag{77}$$

where $2\Lambda/\pi$ is the persistence length. This particular relaxation scenario can be imagined to be the consequence of a sudden temperature jump from finite to zero temperature. Interestingly, the boundary-layer length $\lambda_2(\tau)$ also governs the thermodynamic propagation of tension through semiflexible polymers; e.g., if a weak longitudinal force is suddenly applied at one end [18], or if the polymer is exposed to a shear flow [5].

D. Approximate similarity solutions

As explained in Sec. IV E, type I initial conditions with roughness $\beta<1$ and a large wave number cutoff

$$q_N \gg Q \sim \tau^{-1/4} \tag{78}$$

satisfy the criterion Eq. (40). In this case we can use the right-hand side of Eq. (44) to estimate $\Delta\varrho_l(\tau)$ in Eq. (65),

$$\hat{\zeta}^{-1}\Phi'' \approx \varrho^0(Q)\Delta Q \exp(2\alpha) - \varrho^0, \tag{79}$$

where we approximated

$$\int_{\sqrt{2}Q}^{q_N} dq \varrho^0(q) \overset{q_N\gg Q}{\approx} \int_0^{q_N} dq \varrho^0(q) \equiv \varrho^0, \tag{80}$$

as valid for $\beta<1$. Rather than in the absolute value of Φ we are interested in the ratio

$$\hat{\psi}(s,\tau) \equiv \frac{\Phi(s,\tau)}{\Phi_\infty(\tau)}, \tag{81}$$

where $\Phi_\infty(\tau)$ is the value of Φ in the bulk,

$$\Phi_\infty(\tau) \equiv \lim_{s\to\infty}\Phi(s,\tau). \tag{82}$$

By the definitions Eqs. (81) and (82) $\hat{\psi}(s\to\infty,0)=1$ and $\hat{\psi}(0,\tau)=0$ at the free end to satisfy the boundary condition. As in Sec. IV C, the vanishing of the left-hand side of Eq. (79) in the bulk,

$$0 \approx \varrho^0(Q_\infty)\Delta Q_\infty \exp(2\alpha_\infty) - \varrho^0, \tag{83}$$

implies that the exponent

$$2\alpha_\infty \equiv \frac{\Phi_\infty(\tau)^2}{2\tau} \approx \text{const} \tag{84}$$

is constant in time up to logarithmic corrections. Now we divide Eq. (79) by ϱ^0 and obtain, using Eqs. (81), (83), and (84),

$$2\frac{\sqrt{\alpha_\infty\tau}}{\hat{\zeta}\varrho^0}\hat{\psi}'' = 1 - \frac{\varrho^0(Q)\Delta Q\exp[2\alpha]}{\varrho^0(Q_\infty)\Delta Q_\infty \exp[2\alpha_\infty]}.$$

Inserting the initial conditions Eq. (55) and using the definitions of α, Q, and ΔQ from Sec. IV B, we arrive at

$$2\frac{\sqrt{\alpha_\infty\tau}}{\hat{\zeta}\varrho^0}\hat{\psi}'' = 1 - \hat{\psi}^{-(1+\beta)/2}\exp[2\alpha_\infty(\hat{\psi}^2-1)]. \tag{85}$$

For given α, Eq. (85) is solved by the scaling ansatz

$$\hat{\psi}(s,\tau) = \hat{\psi}\left(\frac{s}{\lambda(\tau)}\right), \tag{86}$$

where the width of the boundary layer is now given by

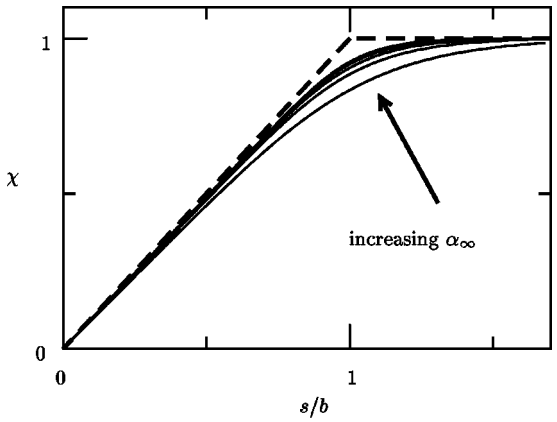

FIG. 11. Type I: Stress profile in the boundary layer, given by the scaling function $\chi(s/\lambda_\beta(\tau))$, Eq. (89). The displayed curves correspond to $\beta=-1$ and $\alpha_\infty=5,10,15,20,25$. For increasing $\alpha_\infty \gg 1$, $\chi(\xi)$ approaches its limiting form $\chi(\xi<1)=\xi$ and $\chi(\xi>1)=1$. The asymptotic behavior is independent of $\beta<1$.

$$\lambda(\tau) \equiv 2(\hat{\zeta}\varrho^0)^{-1/2}(\tau\alpha_\infty)^{1/4}, \tag{87}$$

and thus—in contrast to what we found under type II conditions—is directly proportional to $Q_\infty^{-1}(\tau)$. As the boundary layer width λ_β under type II conditions, it is inversely proportional to $\sqrt{\varrho^0}=O(\epsilon^{1/2})$, which entails the same conclusions as drawn after Eq. (76).

Inserting the scaling form Eq. (86) into Eq. (85) yields

$$\frac{1}{2}\hat{\psi}'(\xi) = 1 - \hat{\psi}^{-(1+\beta)/2}\exp[\alpha_\infty(\hat{\psi}^2-1)]. \tag{88}$$

After solving for $\hat{\psi}(\xi)$ the tension is found as before,

$$\begin{aligned}\varphi(s,\tau) &= \partial_\tau \Phi(s,\tau)\\ &= \sqrt{\frac{\alpha_\infty}{\tau}}\left[\hat{\psi}\left(\frac{s}{\lambda}\right) - \frac{s}{2\lambda}\hat{\psi}'\left(\frac{s}{\lambda}\right)\right]\\ &= \sqrt{\frac{\alpha_\infty}{\tau}}\chi\left(\frac{s}{\lambda(\tau)}\right),\end{aligned} \tag{89}$$

where the normalized scaling function $\chi(\xi)$ is given by

$$\chi(\xi) = \hat{\psi}(\xi) - \frac{1}{2}\xi\hat{\psi}'(\xi). \tag{90}$$

In Fig. 11 the scaling function $\chi(\xi)$ is shown for different $\alpha_\infty>1$. With increasing α_∞ the curves converge from below to a piecewise linear form that consists of a linear boundary layer $\chi(\xi)=\xi$ for $\xi<1$ and a bulk area $\chi(\xi)=1$ for $\xi>1$. This limiting behavior is independent of the exponent $\beta<1$. According to Eq. (65) it corresponds to a completely straightened boundary layer with the linearly growing tension being fully due to the accumulating force from the viscous friction against the solvent, and a buckled bulk regime with a spatially constant pressure conserving its initially stored length. From Eq. (65) it is moreover seen that the limit $\alpha_\infty\to\infty$ physically corresponds to a situation where the region of stored-length release shrinks to a single point at $s=\lambda(\tau)$ that separates the buckled bulk from the relaxed boundary layer. This is in accord with our conclusion at the end of Sec. IV that for type I initial conditions tension decay can be identified with conformational relaxation (see Fig. 8).

From what was said there, we therefore could have guessed the results of the preceding paragraph from an intuitive scaling argument that reverses the above line of arguments. Starting from the very assumption that the rod consists of totally straightened tails of length $\lambda(\tau)$ that dynamically constrain the bulk, one concludes that the bulk pressure $\varphi_\infty(\tau)$ drives the tails outwards at the velocity $v_\parallel$ needed to balance this pressure by the Stokes friction onto the tails, i.e.,

$$\varphi_\infty(\tau) = \hat{\zeta}v_\parallel\lambda(\tau). \tag{91}$$

On the other hand, the velocity of the boundary layer must be equal to the stored-length release per unit of time $v_\parallel = \varrho^0\partial_\tau\lambda$, which takes place in the small crossover region between bulk and boundary layer. Using the power law Eq. (4) for the pressure within the (constrained) bulk with a prefactor $\sqrt{\alpha_\infty}$ we obtain the closed differential equation

$$\varrho^0\hat{\zeta}\lambda\partial_\tau\lambda = \sqrt{\alpha_\infty/\tau}, \tag{92}$$

which is solved by Eq. (87) for the length $\lambda(\tau)$.

E. Consistency

Since both lengths $Q_\infty^{-1}(\tau)$ and $\lambda(\tau)$ grow in time—under type II conditions even with different exponents—one might worry about the time domain of validity of the length scale separation Eq. (61) underlying the above derivation. Consistency of the adiabatic approach requires that the wavelength $Q_\infty^{-1}=(\tau/\alpha_\infty)^{1/4}$ that dominates the sum over all modes is much smaller than the length over which the tension varies, i.e., the width of the boundary layer $\lambda(\tau)$. For type II initial conditions, we thus need

$$Q_\infty(\tau)\lambda_\beta(\tau) = \alpha_\beta^{1/4}\hat{\zeta}^{-1/2}(\Lambda/\tau^{1/4})^{\beta/2-1/2} \gg 1 \tag{93}$$

For $\tau\to 0$ the inequality Eq. (93) is certainly true, because $\beta-1>0$. The product $Q_\infty\lambda_\beta$ becomes comparable to one for $\lambda_\beta(\tau)\approx\Lambda$. However, this point of inconsistency cannot be reached, since we had to assume in the discussion after Eq. (55) that $L\ll\Lambda$ in order to ensure the weakly bending limit. Likewise, for type I initial conditions we need

$$Q_\infty(\tau)\lambda(\tau) = 2[\alpha_\infty/(\hat{\zeta}\varrho^0)]^{1/2} \gg 1. \tag{94}$$

Again, this generally holds in the weakly bending limit Eq. (12).

The adiabatic approximation thus proves to be able to describe the arclength-dependent tension relaxation in the weakly bending limit. On the other hand, the consistency conditions Eqs. (93) and (94) can be taken as another indication that the weakly bending limit is in fact a necessary ingredient for the universality of the relaxation process and in particular for the characteristic power-law relaxation Eq. (4).

F. Terminal relaxation

Up to now, we have considered the growth of the boundary layer in a rod that has a (formally) semi-infinite arclength parameter space, $s=0,\ldots,\infty$, which is an idealization. However, the foregoing discussion obviously applies equally to a free rod of *finite* length L for sufficiently short times: As long as the size of the boundary layer is much smaller than the total length L the presence of a second free end is irrelevant to the boundary layer at the first end. The time where the boundary layers span the whole rod marks the crossover to a new behavior. For definiteness, we define the crossover time τ_f by

$$\lambda(\tau_f) \equiv L. \tag{95}$$

Further contour relaxation proceeds essentially free of lateral stress, because the tension is equilibrated everywhere with the free ends for $\tau \gg \tau_f$. The time τ_f can thus be identified as the characteristic decay time for the tension. From Eqs. (26) and (27) it is seen that after time τ_f all modes decay independently exponentially throughout the whole rod,

$$\varrho(q,\tau > \tau_f) \approx \varrho(q,\tau_f) e^{-q^4(\tau-\tau_f)}. \tag{96}$$

Stored length is no longer conserved, and a mode with wave number q has thus decayed after time $\tau \approx \tau_f + q^{-4}$.

We recall from our discussion at the end of Sec. IV that Eq. (96) corresponds to very different behavior of the overall conformational relaxation for type I and type II initial conditions, respectively. Consider again Fig. 8. In the type I scenario, at τ_f the stored length is concentrated in modes with wavelengths $q^{-1} \approx Q^{-1}(\tau_f)$, which (visibly) dominate the contour undulations. Hence, we can conclude that it takes a time of the order of τ_f to release the bulk of the initially stored length ϱ^0 after the dynamic confinement ceases. In other words, the rod straightens within a time of the order of τ_f. This conforms with the earlier conclusions that tension relaxation and stored-length release occur in parallel, so that the conformation in the boundary layer is the straight ground state.

On the contrary, for type II initial conditions the stored length distribution in mode space hardly differs from the initial condition Eq. (55), i.e. it is still strongly peaked at low q and the total stored length has not changed appreciably. It takes a time $\tau = L^4$ until the contour undulations that carry most of the stored length have relaxed. From the definition, Eq. (95), of τ_f and the boundary layer growth law, Eq. (72), we infer

$$L^4/\tau_f = (\varrho^0)^{-1/(2\delta_\beta)} = O(\epsilon^{-1/(2\delta_\beta)}) \gg 1. \tag{97}$$

The conformational relaxation takes much longer than τ_f, particularly as $\delta_{\beta\to 3} \to 0$. This heralds the (trivial) limit of instant tension equilibration for $\beta \geqslant 3$. As already observed for a confined rod at the end of Sec. IV as well as for the boundary layers discussed in Sec. V C, the conformational relaxation for $\beta > 1$ lags behind the stress relaxation.

We finally comment on the relation to the ordinary perturbation approach of Sec. IV. For free ends, it would to lowest order predict

$$\varphi(s,\tau) = \text{const} = 0. \tag{98}$$

At first sight this contradicts our intuitive understanding that the bulk of a relaxing rod should be under pressure at least for short times. However, fixing the length and time scales L and τ of the problem while $\epsilon \to 0$, the prediction of zero tension is indeed recovered from the adiabatic approach via the vanishing of the relaxation time τ_f in Eq. (95). This is apparent from Eq. (97) for type I initial conditions and from Eq. (87) for type II initial conditions. Thus for any fixed given total length L and time τ there exists an ϵ_c such that the prediction of the multiple-scale perturbation theory reduces to that of the ordinary perturbation scheme for $\epsilon \ll \epsilon_c$. However, the interesting short-time regime $\tau \ll \tau_f(\varepsilon, L)$ is not accessible by ordinary perturbation theory. Upon fixing ϵ and L and considering small $\tau \to 0$ (i.e., the situation just after removing the confining walls that served to keep the tension spatially constant), the decay of the bulk tension obviously has to occur in an arbitrarily narrow boundary region. In other words, the putative $O(\epsilon)$ term f' in Eq. (15b) has to diverge on physical grounds, thus signaling the breakdown of ordinary perturbation theory for open boundary conditions in this limit.

VI. COMPARISON WITH NUMERICAL SIMULATIONS

In this section we want to point out how our results for the stress relaxation manifest themselves in various observables that have been monitored in numerical simulations. Golubovic *et al.* [11] investigated the effect of a sudden temperature jump on an initially straight rod of length l confined between two walls (hinged ends). The frustration due to thermal expansion is modeled by a relative initial compression $\varrho^0 \ll 1$ of the backbone of the rod. The consequent initial pressure φ_i drives the evolution of buckles with wave number $Q_i = \sqrt{\varphi_i/2}$. After a transition period characterized by backbone expansion most of the length $\varrho^0 l$ is stored in bending modes with wave number close to Q_i rather than in backbone vibrational modes. The backbone length appears to be almost constant from there on. The rod relaxes in this second stage as if it was incompressible with a pronounced peak in the initial mode spectrum (prepared by the thermal expansion of the rod). The scenario thus agrees with the assumptions of Sec. IV C. Our analysis there explains why and how the peak grows and sharpens in time. Asymptotically, we predict the dominant wave number to evolve according to $Q \propto \tau^{-1/4}$, as observed in Ref. [11] by analyzing the tangent-tangent correlation function. The fundamental power law Eq. (4) for the tension derived in Sec. IV C is the basis for the power-law time evolution of a number of other observables. For example, the mean-square transverse displacement

$$w^2 \equiv l^{-1} \int_0^l ds r_\perp^2(s,\tau) \tag{99}$$

was observed to obey $w^2 = 2\varrho^0 \tau^{1/2} \propto \tau^{1/2}$ [11] and interpreted as an immediate consequence of the existence of a dominant wavelength, which we established above for type I initial conditions. That is, from the dominance of Q together with the conservation of stored length, one has

$$w^2 = 2\sum_n \varrho(q_n,\tau)q_n^{-2} \approx 2\varrho(Q,\tau)Q^{-2} = 2\varrho^0 Q^{-2} \sim \tau^{1/2}. \tag{100}$$

Analogous arguments can be used for other observed quantities, such as the stored elastic energy or the dissipation rate, etc. Moreover, as we have shown in Secs. IV B and IV C, the cascading of stored length in mode space maintains and enhances the maximum in the mode spectrum asymptotically, even if the initial mode spectrum has a (slowly) decaying form. The validity of Eq. (100) and the related power-law behavior of other observables thus also extend to this situation.

The simulations by Spakowitz and Wang [12] considered the same setup as in Ref. [11] but with free boundary conditions. In addition to a higher-order effect guiding the evolution of helical modes, the same power laws are found for the dominant wave number and the evolution of transverse displacements, respectively. This becomes more easily comprehensible from our boundary-layer calculations, which show that most of the rod should indeed behave as if it were longitudinally confined as long as the boundary layer does not span the whole filament, e.g., for $\tau \ll \tau_f$. Additionally, as a measure for the longitudinal expansion Spakowitz and Wang [12] proposed a longitudinal radius of gyration $R_\parallel^G$ as the largest eigenvalue of a gyration tensor. In our terms, this quantity can be identified with

$$R_{G\parallel}^2(\tau) \equiv \frac{1}{L}\int_0^L ds[z_{CM} - s + r_\parallel(s,\tau)]^2 \tag{101}$$

for a rod with a time-independent longitudinal center of mass coordinate $z_{CM}=s_{CM}-r_\parallel(s_{CM})$ lying approximately at the center of the rod,

$$z_{CM} + r_\parallel(0) \approx L/2. \tag{102}$$

Using the arguments developed above, the time derivative $\partial_\tau R_{G\parallel}^2(\tau)$ is in the limit $\tau \to 0$ given by

$$R_{G\parallel}\partial_\tau R_{G\parallel} = \frac{1}{L}\int_0^L ds[z_{CM} - s + r_\parallel]_{\tau=0}\partial_\tau r_\parallel$$

$$\approx \int_0^{L/2} ds \partial_\tau r_\parallel \tag{103a}$$

$$= \int_0^{L/2} ds \int_0^s ds' \partial_\tau \varrho(s',t) \tag{103b}$$

$$= \hat{\zeta}^{-1}\varphi_\infty \propto \tau^{-1/2}. \tag{103c}$$

The first approximation Eq. (103a) follows from Eq. (102) and from the fact that for short times $\partial_\tau r_\parallel$ is finite (to leading order) only close to the ends, $s=0$ and $s=L$. Equation (103c) holds because of $\partial_t \varrho = \varphi''/\hat{\zeta}$ after differentiating Eq. (64) with respect to time. Integrating Eq. (103) in time and observing $R_\parallel^G(0) \approx L/(2\sqrt{3})$ one gets the algebraic growth law

$$\delta R_\parallel^G(\tau) \equiv R_\parallel^G(\tau) - R_\parallel^G(0) \propto \tau^{1/2}, \tag{104}$$

which is indeed empirically found to hold with high accuracy over a broad time window [12]. Note, however, that according to Eq. (103) this (initial) variation of the radius of gyration measures the time integral of the bulk tension rather than the growth of the boundary layer. It thus provides a practical direct measure of $\Phi(\tau)$, but is not suitable to monitor the conformational relaxation.

Access to the latter can be gained by probing the end-to-end distance

$$R_\parallel = L - r_\parallel(L) + r_\parallel(0) \tag{105}$$

instead. Its temporal change $\delta R_\parallel(\tau) \equiv R_\parallel(\tau) - R_\parallel(0)$ is obviously directly due to stored-length release. Under type I conditions, where stored-length release and tension decay go hand in hand and the boundary layer is essentially straight, the released length is nothing but the total stored length that was initially contained in the boundary layer, i.e.,

$$\delta R_\parallel(\tau) \approx \varrho^0 \lambda(\tau) \propto \sqrt{\varrho^0}\tau^{1/4}. \tag{106}$$

Rods with type II initial conditions behave differently. Again, stored-length release does not occur in the bulk. However, the stored length in the boundary layer is released much more slowly than the boundary layer grows, as discussed in Sec. V F. Not all of the initially stored length but only some fraction $\Delta\varrho^*(q,\tau)$ has been released after time τ. The latter can be estimated from Eq. (96), since the relaxation within the boundary layer is essentially tension-free:

$$\Delta\varrho^*(q,\tau) = \int_{L^{-1}}^\infty dq \varrho^0(q)(e^{-q^4\tau} - 1) \overset{\tau^{1/4} \ll L}{\sim} \Lambda^{1-\beta}\tau^{(\beta-1)/4}. \tag{107}$$

Asymptotically we can thus write

$$\delta R_\parallel(\tau) \approx \Delta\varrho_\beta^*(\tau)\lambda_\beta(\tau) \propto \sqrt{\varrho^0}\tau^{(\beta-1)/4+\delta_\beta}, \tag{108}$$

for short times $\tau \ll \tau_f$. In the last step we used $\Lambda^{1-\beta} \propto \varrho^0$ from Eq. (57). For $\tau \approx \tau_f$ the growth of the boundary layer saturates at $\lambda \simeq L$, so that for long times $\tau \gg \tau_f$

$$\delta R_\parallel(\tau) \approx \Delta\varrho_\beta^*(\tau)L \propto \varrho^0\tau^{(\beta-1)/4}. \tag{109}$$

In summary, for type II initial conditions

$$\delta R_\parallel(\tau) \propto \begin{cases} \sqrt{\varrho^0}\tau^{\gamma_\beta^<}, & \gamma_\beta^< = \dfrac{\beta+1}{8} \quad (\tau \ll \tau_f), \\ \varrho^0\tau^{\gamma_\beta^>}, & \gamma_\beta^> = \dfrac{\beta-1}{4} \quad (\tau \gg \tau_f). \end{cases} \tag{110}$$

In particular, we note that an initially thermalized rod first expands according to $\delta R_\parallel \propto \tau^{3/8}$ and eventually as $\delta R_\parallel \propto \tau^{1/4}$. The exponents $\gamma_\beta^<$ and $\gamma_\beta^>$, which obey $\gamma_\beta^< = \gamma_\beta^> + \delta$, are displayed in Fig. 12 together with δ_β for comparison.

The initial growth laws Eqs. (106) and (108) including prefactors can also be derived more rigorously from the scaling forms for the integrated tension derived in Secs. V C and V D For type I initial conditions $\Delta\varrho(s,\tau)/\varrho^0$ is given by the right-hand side of Eq. (85); hence

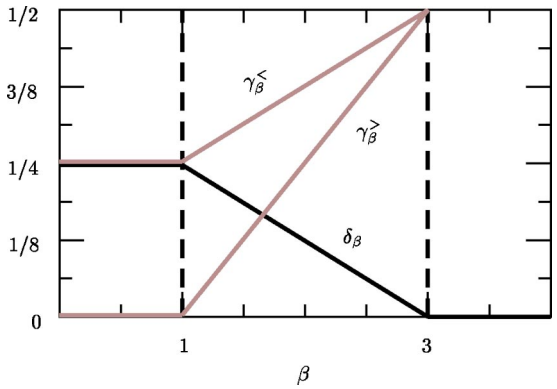

FIG. 12. The exponents $\gamma_\beta^<$ and $\gamma_\beta^>$ (grey) determine the growth $\delta R_\parallel \propto \tau^{\gamma_\beta}$ for the end-to-end distance on short ($\tau \ll \tau_f$) and long times ($\tau \gg \tau_f$), respectively. The exponent $\delta_\beta = \gamma_\beta^< - \gamma_\beta^>$ (black) characterizes the growth $\lambda_\beta \sim \tau^{\delta_\beta}$ of the width of the boundary layer.

$$\begin{aligned}\delta R_\parallel(\tau) &= 2\int_0^\infty ds \Delta\varrho(s,\tau)\\ &= 2\int_0^\infty ds \varrho^0(1-\hat{\psi}^{-(1+\beta)/2}\exp\{2\alpha_\infty[\hat{\psi}^2(s,\tau)-1]\})\\ &= \lambda(\tau)\varrho^0\int_0^\infty d\xi(1-\hat{\psi}^{-(1+\beta)/2}\exp\{2\alpha_\infty[\hat{\psi}^2(\xi)-1]\})\\ &\propto \sqrt{\varrho^0}\tau^{1/4}. \end{aligned} \tag{111}$$

The exact prefactor can be obtained as a function of the appropriate scaling function by evaluating the integral numerically. For type II initial conditions one finds

$$\begin{aligned}\delta R_\parallel(\tau) &= 2\int_0^\infty ds \Delta\varrho(s,\tau)\\ &= 2\int_0^\infty ds \Lambda^{1-\beta}\int_0^\infty dq q^{-\beta}[e^{2q^2[\Phi(s,\tau)-q^2\tau]}-1]\\ &= \Lambda^{1-\beta}\tau^{(\beta-1)/4}\lambda_\beta(\tau)\int_0^\infty d\xi 2\int_0^\infty dq q^{-\beta}[e^{2q^2[\psi(\xi)-q^2]}-1]\\ &\propto \sqrt{\varrho^0}\tau^{\gamma_\beta}, \end{aligned} \tag{112}$$

which also gives an explicit expression for the prefactor in terms of the scaling function $\psi(\xi)$.

We finally comment on a possible problem that could arise because of the "microscopic" nature of $\delta R_\parallel$. Note that, in contrast to $\delta R_\parallel^G$, it is also sensitive to microscopic details of the relaxation and the initial conditions, since it contains contributions from Fourier modes beyond those corresponding to the coarse-graining length l. In particular, the longitudinal projection of transverse fluctuations near the ends could possibly mix into the genuinely longitudinal dynamics, thereby affecting the observed time dependence. This effect plays indeed an important role for the longitudinal fluctuations and linear response of stiff polymers pulled at their ends [2,18]. The situation is somewhat more fortunate in the present case, since one can show the "microscopic" contributions to obey the same power-law dynamics but with a prefactor of lower order in ϵ.

Altogether, it appears that evidence for the bulk relaxation of type I initial conditions, i.e., in the regime of mode-space localization corresponding to $\beta<1$, can be found in existing simulations. The more complicated intermediate asymptotic regime for type II initial conditions and our predictions for the boundary-layer dynamics represent interesting additional features, which could be verified in simulations by probing the growth of the end-to-end distance. Finally, we anticipate a result of ongoing work [15] in which we include thermal noise in our considerations. The power laws (not the prefactors) derived here for a deterministic rod with $\beta=2$ turn out to describe the physics of a semiflexible polymer after a sudden change in persistence length. (The latter may be experimentally realized by addition of chemicals rather than by a sudden temperature quench.) Thus, semiflexible polymers may lend themselves to an experimental investigation of our scaling predictions for the particular case $\beta=2$. After this work was completed, we learned about related work by Bhobot-Raviv *et al.* [22] for DNA.

VII. CONCLUSIONS AND OUTLOOK

We have developed and applied in Sec. V and the Appendix an adiabatic method to calculate the overdamped heterogeneous stress relaxation in a multiply but weakly buckled rod. The possible generic relaxation scenarios could conveniently be characterized in terms of an exponent β characterizing the roughness of the initial contour. The coarse-grained pressure $\varphi_l(s,\tau)$ along the rod backbone could be cast into the universal scaling form

$$\varphi_l(s,\tau) = \sqrt{\frac{\alpha_\beta}{\tau}}\chi_\beta\left(\frac{s}{\lambda_\beta(\tau)}\right), \tag{113}$$

with a boundary-layer width

$$\lambda_\beta(\tau) \sim \tau^{\delta_\beta}, \tag{114}$$

and a normalized monotone scaling function $\chi_\beta(\xi)$,

$$\chi_\beta(\text{end}) = 0,\ \chi_\beta(\text{bulk}) = 1.$$

The latter was calculated numerically and displayed in Figs. 10 and 11 for the two fundamentally different cases $\beta<1$ (type I) and $1<\beta<3$ (type II), respectively. The amplitude $\sqrt{\alpha_\beta}$ of the power-law decay of the tension in the bulk depends on the initial conditions as summarized by Fig. 7. The exponent δ_β depicted in Fig. 12 characterizes the growth of the width of the boundary layer over which the tension continuously decays from its bulk value $\sqrt{\alpha_\beta/\tau}$ to zero. The particular case of thermal initial conditions corresponds to $\sqrt{\alpha_{\beta=2}} \approx 0.386$ and $\lambda_{\beta=2}=1/8$. For type I initial conditions the dynamics is governed by a unique characteristic dynamic length scale Q^{-1}. Tension propagation coincides with contour relaxation. The contour has relaxed by the time τ_f when the tension has equilibrated throughout the rod. On the contrary, for type II initial conditions, the boundary-layer width constitutes an additional dynamic length scale that behaves dif-

ferently from Q^{-1}. Tension relaxation precedes contour relaxation and most of the contour relaxation occurs under negligible tension.

From these central results we derived corresponding power laws for a number of observables that seem well suited to test our predictions in simulations. In particular, we showed that the longitudinal radius of gyration $R_{\parallel}^{G}$ is suitable to directly probe the (universal) tension relaxation in the bulk, i.e., the prefactor in Eq. (113). The more complex boundary-layer growth Eq. (114), which sensitively depends on the type of initial conditions, was shown to be reflected in the conformational dynamics. It can be accessed by a measurement of the longitudinal end-to-end distance $R_{\parallel}$, which was predicted to exhibit the intriguing dynamical crossover behavior summarized in Eq. (110).

Following Spakowitz and Wang [12], an interesting route for future theoretical investigations could be to allow for higher order contributions to the harmonic wormlike-chain Hamiltonian in Eq. (1) to analyze the intriguing nonlinear phenomenon of helix formation and coarsening.

With minor modifications the adiabatic method developed here can be used to determine stress profiles for nondeterministic, thermal dynamics (i.e., for semiflexible polymers in various situations of external driving), and will thus be helpful in establishing a unified description of tension propagation in stiff polymers. In fact, even the athermal case considered here can for the special choice $\beta=2$ be interpreted as a special nonequilibrium thermodynamics problem: the free contour relaxation after a sudden temperature jump in the limit of vanishing final temperature. The above derived scaling behavior (but not the amplitudes) can be shown to generalize to the case that the final temperature is finite [15].

ACKNOWLEDGMENTS

We gratefully acknowledge helpful discussions with Jan Wilhelm during the early stages of this work.

APPENDIX: METHOD OF MULTIPLE SCALES

Given the separation of the length scales Q^{-1} and λ observed in Sec. V A, it is natural to apply the method of multiple scales [21] to find an approximate closed equation for the slow variation of the tension $\varphi(s,\tau)$ over the length scale λ that is independent of the detailed "microscopic" fluctuations on the scale Q^{-1}. To this end, we introduce rapidly and a slowly varying arclength coordinates, $x\equiv s$ and $y\equiv s\epsilon^{\alpha}$, respectively, where the exponent $\alpha>0$ will be fixed later. Any function $g(s)$ depending on the arclength s is now considered to depend on both variables $g(s)\to g(x,y)$, where x and y are treated as independent. The original arclength derivative then becomes

$$\partial_s|_{\tau} \equiv \partial_x|_{\tau,y} + \epsilon^{\alpha}\,\partial_y|_{\tau,x}. \tag{A1}$$

The dynamic variables $r_{\perp}$ and $f=\kappa\varphi$ in the equations of motion Eqs. (15) are assumed to have a uniform power expansion (the expansion coefficients in each order have to be bounded [21]) in terms of the small parameter ϵ,

$$\mathbf{r}_{\perp} = \epsilon^{1/2}\mathbf{h}_0 + o(\epsilon^{1/2}),$$

$$\varphi = \varphi_0 + \epsilon\varphi_1 + o(\epsilon). \tag{A2}$$

Eliminating the (dependent) coordinate $r_{\parallel}$ via the local constraint Eq. (13) to the required order and inserting the power expansions Eq. (A2) in the equations of motion yields

$$\mathbf{0} = \epsilon^{1/2}[\partial_{\tau}\mathbf{h}_0 + \partial_x^4\mathbf{h}_0 + \partial_x(\varphi_0\partial_x\mathbf{h}_0)] + o(\epsilon^{1/2}), \tag{A3a}$$

$$0 = \partial_x^2\varphi_0 + \epsilon^{\alpha}2\partial_x\partial_y\varphi_0 + \epsilon^{2\alpha}\partial_y^2\varphi_0 + \epsilon[\partial_x^2\varphi_1 - X_0(x,y)] + o(\epsilon;\epsilon^{2\alpha}). \tag{A3b}$$

By

$$X_0(x,y) = \frac{\hat{\zeta}}{2}\partial_{\tau}(\partial_x\mathbf{h}_0)^2 + \frac{1}{2}\partial_x^2[\varphi_0(\partial_x\mathbf{h}_0)^2] + \frac{1}{2}\partial_x^4(\partial_x\mathbf{h}_0)^2 - (1-\hat{\zeta})\partial_x[(\partial_x\mathbf{h}_0)(\partial_{\tau}\mathbf{h}_0)],$$

we have summarized terms nonlinear in $\mathbf{h}_0$. The $O(1)$ part of Eq. (A3b) together with the requirement of φ_0 being bounded for large x imply that

$$\varphi_0(x,y) = \hat{\varphi}_0(y) \tag{A4}$$

is independent of x, so that the $O(1)$ and $O(\epsilon^{\alpha})$ terms of Eq. (A3b) vanish. The leading order in this equation could therefore be either $O(\epsilon^{2\alpha})$ or $O(\epsilon)$. With Eq. (A4) we can solve the $O(\epsilon^{1/2})$ part of Eq. (A3a) for $\mathbf{h}_0(x,y)$ in terms of Fourier modes of the variable x along the lines of Sec. IV B and use the result to evaluate $X_0(x,y)$. It then turns out that the first term in X_0 implies that φ_1 would have to grow without bound with increasing system size (secular term), if the $O(\epsilon)$ terms alone were required to cancel each other. However, the nonlinear term can also be balanced by the $O(\epsilon^{2\alpha})$ term after choosing $\alpha=1/2$; i.e., the exponent α is fixed such that the expansion coefficient φ_1 remains bounded.[4] The equation fixing φ_1 then reads

$$\partial_x^2\varphi_1(x,y) + \partial_y^2\hat{\varphi}_0(y) = X_0(x,y). \tag{A5}$$

The balance of the secular terms implies the balance of the x averages of their derivatives that appear in Eq. (A5), where x averaging is defined by

$$\langle g(x,y)\rangle_x(y) = \lim_{l\to\infty}\int_0^l \frac{dx}{l}g(x,y). \tag{A6}$$

Note that x averages of terms that are total derivatives of bounded (nonsecular) quantities with respect to x all vanish upon formally taking the coarse-graining length $l\to\infty$ in Eq. (A6), so that we are left with

[4]The small parameter $\epsilon^{\alpha}=\epsilon^{1/2}$ appearing here is the same as in the length scale separation Eq. (60) observed in Sec. V A.

$$\partial_y^2 \hat{\varphi}_0(y) = \frac{\hat{\zeta}}{2} \langle \partial_\tau (\partial_x \mathbf{h}_0)^2 \rangle_x(y). \tag{A7}$$

For the finite rod under consideration, the limit $l \to \infty$ is not to be taken literally though. Rather, the average in Eq. (A6) is required to become independent of l to leading order in ϵ for l much smaller than the system size. For the quantities of interest this was already established in Sec. V B. Therfore, we can identify Eq. (A7) with the coarse-grained equation Eq. (65). Relating corresponding quantities, $\hat{\varphi}_0(y)$ which depends only on the slow variable y is recognized as the former coarse-grained tension $\varphi_l(s)$, while the x-averaged expansion coefficient $\langle \varphi_1(x,y) \rangle_x = \hat{\varphi}_1(y)$ corresponds to the time derivative $\partial_\tau \epsilon_l(s)$ of the coarse-grained stored length.

[1] J. Wilhelm and E. Frey, Phys. Rev. Lett. **77**, 2581 (1996).
[2] L. Le Goff, O. Hallatschek, E. Frey, and F. Amblard, Phys. Rev. Lett. **89**, 258101 (2002).
[3] C. H. Wiggins, D. X. Riveline, A. Ott, and R. E. Goldstein, Biophys. J. **74**, 1043 (1998).
[4] D. Moldovan, and L. Golubović, Phys. Rev. Lett. **82**, 2884 (1999).
[5] V. Shankar, M. Pasquali, and D. C. Morse, J. Rheol. **46**, 1111 (2002).
[6] M. L. Gadel, M. T. Valentine, J. C. Crocker, A. R. Bausch, and D. A. Weitz, Phys. Rev. Lett. **91**, 158302 (2003).
[7] L. D. Landau and E. M. Lifshitz, *Theory of Elasticity*, Course of Theoretical Physics Vol. 7 (Pergamon, London, 1959).
[8] U. Seifert, W. Wintz, and P. Nelson, Phys. Rev. Lett. **77**, 5389 (1996).
[9] A. Ajdari, F. Jülicher, and A. Maggs, J. Phys. I **7**, 823 (1997).
[10] P. Ranjith and S. Kumar, Phys. Rev. Lett. **89**, 018302 (2002).
[11] L. Golubović, D. Moldovan, and A. Peredera, Phys. Rev. Lett. **81**, 3387 (1998); Phys. Rev. E **61**, 1703 (2000).
[12] A. J. Spakowitz and Z. G. Wang, Phys. Rev. E **64**, 061802 (2001).
[13] M. Doi, and S. F. Edwards, *The Theory of Polymer Dynamics* (Clarendon, Oxford, 1986).
[14] H. Yamakawa, *Modern Theory of Polymer Solutions* (Harper & Row, New York, 1971).
[15] O. Hallatschek, E. Frey, and K. Kroy, e-print cond-mat/0405367.
[16] J. Cahn and J. Hilliard, J. Chem. Phys. **28**, 258 (1958).
[17] A. Bray, Adv. Phys. **43**, 357 (1994).
[18] R. Everaers, F.Jülicher, A. Ajdari, and A. C. Maggs, Phys. Rev. Lett. **82**, 3717 (1999).
[19] R. E. Goldstein and S. A. Langer, Phys. Rev. Lett. **75**, 1094 (1995).
[20] C. H. Wiggins, A. Montesi, and M. Pasquali, e-print cond-mat/0307551.
[21] M. H. Holmes, *Introduction to Perturbation Methods* (Springer, New York, 1995), Chap. 5.
[22] Y. Bhobot-Raviv, W. Z. Zhao, M. Feingold, C. H. Wiggins, and R. Granek, Phys. Rev. Lett. **92**, 098101 (2004).